Journal of
Medicinal Chemistry

Article

Platinum-Based Modification of Styrylbenzylsulfones as Multifunctional Antitumor Agents: Targeting RAS-RAF Pathway, Enhancing Antitumor Activity and Overcoming Multidrug Resistance

Zhikun Liu, Meng Wang, Heng-Shan Wang, Lei Fang, and Shaohua Gou

J. Med. Chem., **Just Accepted Manuscript** • DOI: 10.1021/acs.jmedchem.9b01223 • Publication Date (Web): 10 Dec 2019

Just Accepted

is published by the American Chemical Society. 1155 Sixteenth Street N.W., Washington, DC 20036

Platinum-Based Modification of Styrylbenzylsulfones as Multifunctional Antitumor Agents: Targeting RAS-RAF Pathway, Enhancing Antitumor Activity and Overcoming Multidrug Resistance

Zhikun Liu[a,1], Meng Wang[b,1], Hengshan Wang[b], Lei Fang[a,*], Shaohua Gou[a,*]

[a] *Jiangsu Province Hi-Tech Key Laboratory for Biomedical Research, Southeast University, Nanjing, 211189, China*

[b] *State Key Laboratory for the Chemistry and Molecular Engineering of Medicinal Resources, School of Chemistry and Pharmaceutical Sciences of Guangxi Normal University, Guilin, 541004, China*

[1]These authors contributed equally.

[*] Corresponding authors

E-mail: lei.fang@seu.edu.cn (L. Fang); sgou@seu.edu.cn (S. Gou)

ABSTRACT: Inhibiting/disturbing the RAS-RAF pathway may benefit the treatment of cancer and overcome the resistance. Utilizing such pathway as the target, nine styrylbenzylsulfone derivatives generated from the platinum-based modification of the side chain of Rigosertib were designed. Among them, compound **29** showed the most potent antitumor activity in vitro with IC_{50} values at nanomolar level against the tested tumor cell lines and 1000-fold higher than cisplatin against the multidrug resistant cells (A549/CDDP, A549/DOX, and SKOV-3/CDDP cells) while showed only moderate cytotoxicity against normal cells (HEUVC cells). Compound **29** could clearly disturb signaling transduction between RAS and CRAF by directly bonding to CRAF and inhibit CRAF activation. Besides, the enhanced intracellular platinum level made **29** more potent than cisplatin in DNA damage, ROS accumulation and mitochondrial membrane potential decrease. Moreover, **29** induced apoptosis by endogenous pathway and efficiently inhibited tumor growth in A549 xenograft model without side effect.

Key Words: overcoming multidrug resistance, RAS-CRAF interference agent, drug conjugation

INTRODUCTION

The mitogen-activated protein kinase (MAPK) signaling pathway is of great importance to cellular biological functions, which not only activates proliferative signals but also affects signals that are responsible for differentiation and apoptosis [1-3]. The signal transmission is achieved by

the conversation from RAS.GDP (inactive) to RAS.GTP (active) with the help of extracellular signals and in turn triggering several downstream cascades, including RAF-MEK-ERK pathway [4]. Naturally, the MAPK pathway was frequently dysregulated in many cancers harboring RAS mutations, resulting in constitutive activation of the pathway, uncontrolled proliferation and decreased cellular sensitivity to agents that could originally induce apoptosis [5-7]. Therefore, it will be attractive to inhibit the activation of RAS for the treatment of cancers. However, the lack of well-defined druggable pockets and cavities on the RAS surface made RAS an 'undruggable' target [8-10]. In addition, the RAS genes in cancer cells mutated frequently, which made inhibition of RAS activation directly more challenging. Thus, alternatively, disturbing the signal transduction between RAS proteins and downstream effectors could serve as a new approach to develop novel RAS-driven therapies.

In mammals, RAF family contains three members: ARAF, BRAF and CRAF, binding with RAS as upstream activator and mediating the MAPK signaling transduction to the MEK as only downstream effector. Among those three subtypes, CRAF plays an important role as a mediator in mutant KRAS-driven proliferation and tumor development [11]. On the other hand, CRAF also affects the anti-tumor activity of BRAF inhibitors and MEK feedback-mediated pathway [12-14]. Therefore, in consideration of inhibiting signaling transduction of RAS, inhibition of CRAF activation was proved to be an effective method to disturb RAS-driven tumorigenesis and feedback reactivation [15]. Rigosertib (**Figure 1**) belongs to the benzylstyryl sulphone compounds and can inhibit tumor cell proliferation in nanamole ranges, including some resistant cells [16, 17]. In in vitro study, Rigosertib acted as RAS analogues to bind to RAS effectors, resulting in their inability to bind to RAS, disrupting RAF activation, and inhibiting activation of the RAS-RAF-MEK pathway [16].

From the structure-activity relationship point of view, the nature, number, and position of substituents on the two aromatic rings of Rigosertib, as described by Reddy et al. [16], are conservative and cannot tolerate significant structural modification. Thus, we have paid attention to the carboxyl group at the end of the side chain. In the past, the therapeutic potential of metal-based complexes has been widely used and investigated for cancer therapy, because of the unique characteristics of metals, such as redox activity, lewis acid properties and reactivity toward the organic substrate [18]. A large number of metal-based complexes have been designed and

synthesized and among them several complexes were proved to be promising anticancer agents. For example, Ma et al. found a novel benzofuran-conjugated iridium(III) complex as a STAT3 and NF-kB dual inhibitor in prostate cancer cells [19]. Leung et al. found an enantiomeric iridium(III) metal-based compound as an efficient RAS/RAF interaction inhibitor, which could directly engage both H-Ras and Raf-1-RBD and efficiently disrupt the signaling between RAF/RAF/MEK/ERK [20]. Zhang et al. also summarized chirality metal-based agents in cancer research [21]. Therefore, metal-based complexes in cancer therapy has attracted a lot of interest. Platinum drugs, such as cisplatin (CDDP), carboplatin and oxaliplatin (**Figure 1**), have been developed into an important part of clinical chemotherapy. As a kind of cytotoxic agents, platinum drugs mainly act on DNA and then cause death of tumor cells. This action mechanism is quite different from that of Rigosertib, suggesting introduction of platinum pharmacophore to Rigosertib may give additional activity to the parent compound. On the other hand, the platinum drugs often suffer from the severe toxic side effects and the acquired resistance associated with the long-term application [22-27]. Given the good performance of RAS inhibitors against the multiple-resistance tumor cells, it may be anticipated that combination of Rigosertib and platinum drugs may overcome the resistance.

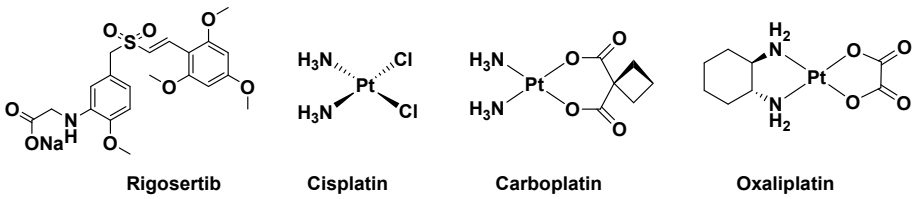

Figure 1. Structures of Rigosertib and current Pt(II) drugs approved for worldwide use.

In this context, we here made structural modifications to Rigosertib by conjugating a platinum(IV) complex, which can be considered as a stable prodrug of the classic platinum(II) drug [28, 29], to carboxyl group via different linkers. The resulting conjugates were supposed to be relative stable under the circulation condition, and the good lipophilicity [30, 31], as compared with the traditional platinum(II) complex, could be beneficial for the uptake by tumor cells. When entering the tumor cells, the conjugates could be effectively reduced by the reductive substances (e.g. glutathione, protein and other biomoleculesn [28-32]) in tumor cells to release Rigosertib and platinum(II) complex to exert anti-tumor activity via different pathways. Thus, enhancing activity and the potential to overcome the multidrug resistance can be expected. Our drug design idea is

outlined in **Figure 2**.

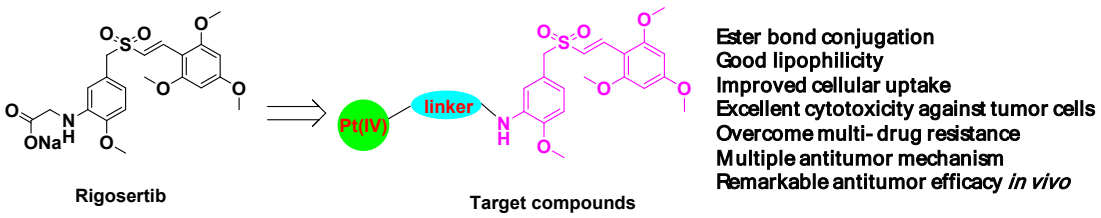

Figure 2. The structural modification strategy and the drug design idea of the target compounds.

RESULTS AND DISCUSSION

Chemistry. As shown in **Scheme 1** and **2**, compound **8** was prepared according to previously reported procedures [16], which was further esterified and followed by a hydrolysis reaction to give compounds **13** and **14**. Pt(IV) complexes **15, 16** and **17** were obtained by oxidation of the corresponding Pt(II) complexes following known procedures [32-34]. As for the synthesis of compound **26** (carboxyl acid form of Rigosertib), compound **8** was firstly treated with ethyl bromoacetate and then hydrolyzed to offer **26** in high yield. Finally, nine Pt(IV) derivatives were obtained via combining **15**, **16** or **17** with compounds **13, 14** and **26,** respectively, in the presence of O-(benzotriazol-1-yl)-N,N,N',N' -tetramethyluronium tetrafluoroborate (TBTU). All of the target compounds were characterized with ^{1}H-NMR, ^{13}C-NMR and ESI-MS techniques.

Scheme 1. Preparation of Pt(IV) Complexes 18-23

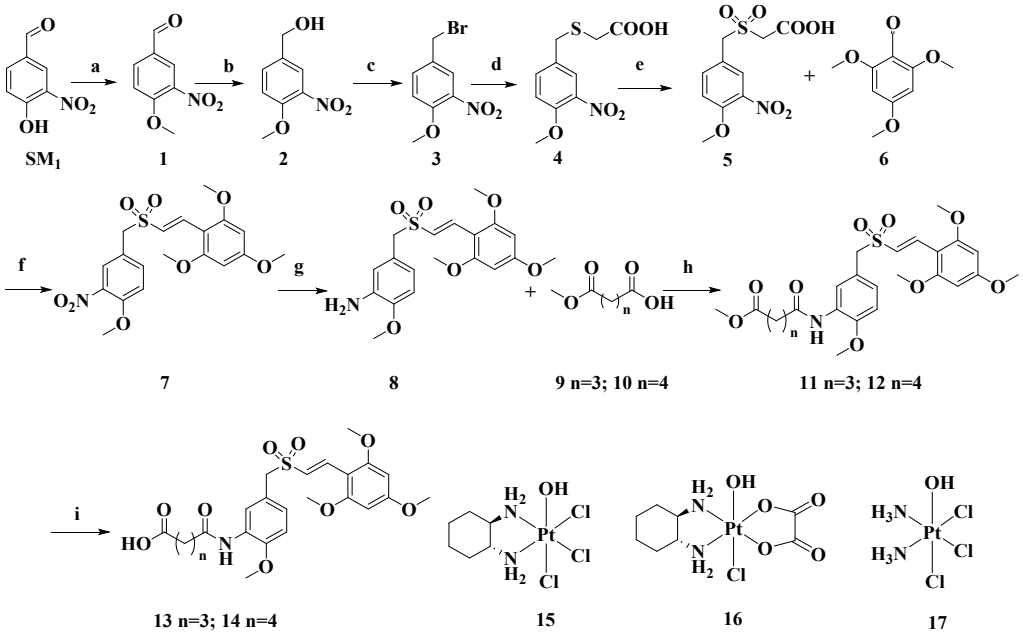

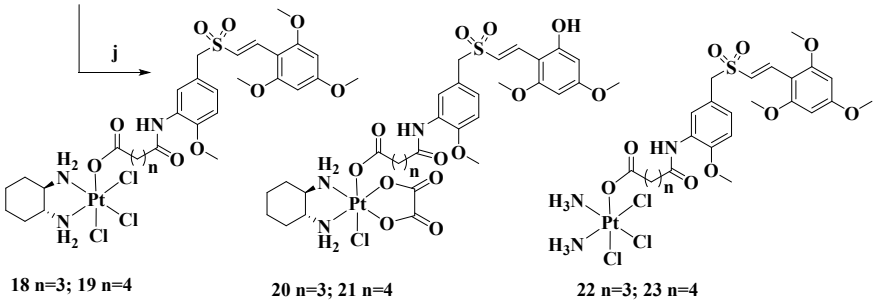

Reagents and conditions: a) CH_3I, K_2CO_3, DMF; b) $NaBH_4$, MeOH; c) PBr_3, DCM; d) Mercapto acetic acid, NaOH, MeOH; e) H_2O_2, AcOH; f) Piperidine, benzoic acid, toluene; g) Fe, NH_4Cl, EtOH, H_2O; h) Oxalyl chloride, Et_3N, DCM; i) LiOH•H_2O, CH_3OH, H_2O; j) TBTU, Et_3N, **15**/**16**/**17**, DMF.

Scheme 2. Preparation of Pt(IV) Complexes 27-29

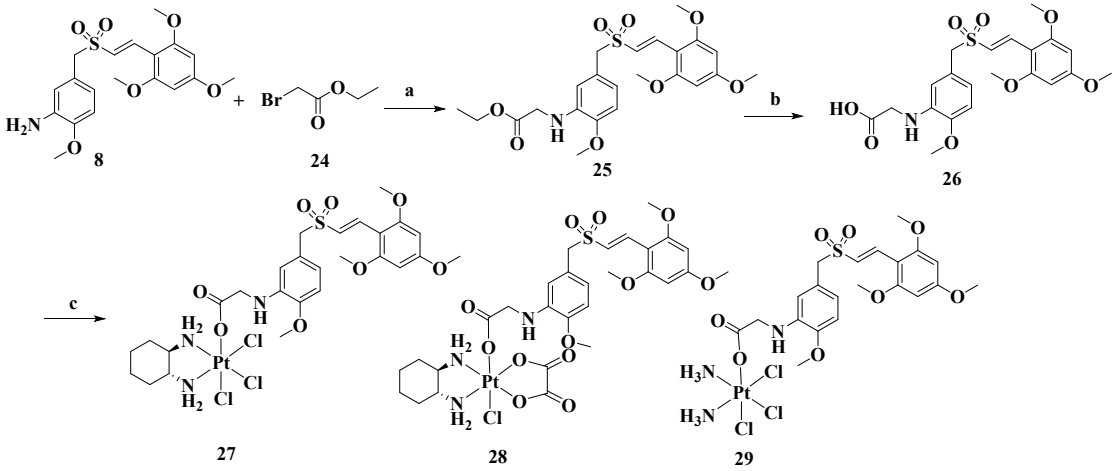

Reagents and conditions: a) K_2CO_3, KI, DMF; b) LiOH•H_2O, CH_3OH, H_2O; c) **15/16/17**, TBTU, Et_3N, DMF.

In Vitro Cytotoxicity Measurement. The cytotoxicity of the synthesized target compounds was evaluated by MTT methods, using **26** (carboxyl acid form of Rigosertib), cisplatin and oxaliplatin as references. Different cancer cell lines, including A549 (non-small cell lung cancer cell line), MGC-803 (gastric cancer cell line), SKOV-3 (ovarian cancer cell line), and NCI-H460 (large cell lung cancer cell line) were used in this study. The results after 72 h drug exposure were shown in **Table 1**. All of these compounds tested showed moderate to strong anti-proliferative activity against the cancer cells. It was found that the cytotoxicity of **19, 21** and **23** containing a four methylene linker was higher than that of **18, 20** and **22** owning a three methylene linker, but their IC_{50} values are only at the level of cisplatin and oxaliplatin. Interestingly, when a glycine group was employed as the linker, the resulting complexes (i.e. **27**, **28**, **29**) showed much better activity than the above mentioned compounds. It was observed that all cancer cell lines tested

were sensitive to complexes **27-29** with the IC_{50} values comparable to those of compound **26**, but much lower than those of cisplatin and oxaliplatin. Since the target complexes can be regarded as prodrugs, we assumed that the original styrylbenzylsulfone moiety was mainly responsible for their antitumor activity. Complexes **27-29** were capable of releasing **26**, a known potent antitumor agent. In contrast, complexes **18-23** were capable of releasing compounds **13** or **14**. Our MTT assay revealed that **13** or **14** showed only moderate cytotoxic activity with IC_{50} values ranged from 10.81-17.31 μM against the tested tumor cells (**Table 1**), much lower than **26** whose IC_{50} values ranged from 44-83 nM. Thus, it may be understandable why complexes **27-29** showed much better activity.

Among all of the target compounds, **29** showed the best activity, with the potency at least over 1000-fold higher than cisplatin and even 10-fold higher than **26** against A549. In contrast, the combination administration of **26** with cisplatin (i.e. equal molar **26**/cisplatin mixture) didn't show significant improvement of the activity relative to the administration of **26** alone. Unexpectedly, compound **8** showed low cytotoxicity against these cancer cell lines tested, which may be attributed to the miss of the glycine group as well as its poor solubility in aqueous buffers and solutions [16]. However, when the amino group was converted to glycine, the resulting compound **26** produced much better cytotoxic activity than compound **8** against all cancer cells used in this study. The enhanced activity of **26** illustrated that the glycine group was of great importance for the anti-proliferative activity.

Table 1. IC_{50} values of the tested compounds toward various cancer cell lines.

Compd.	[a]IC50 (μM)			
	A549	MGC-803	SKOV-3	NCI-H460
8	>50	>50	>50	>50
13	10.81 ± 1.24	13.96 ± 1.23	17.31 ± 1.32	15.14 ± 0.38
14	13.82 ± 1.75	12.58 ± 1.67	14.58 ± 1.43	14.28 ± 1.12
18	10.09 ± 0.83	5.70 ± 0.19	2.88 ± 0.11	16.40 ± 1.13
19	6.91 ± 0.63	6.57 ± 0.25	2.81 ± 0.04	16.33 ± 1.12
20	19.50 ± 1.18	4.03 ± 0.23	6.53 ± 0.32	23.39 ± 1.78
21	16.75 ± 0.88	4.68 ± 0.34	5.87± 0.25	13.99 ± 0.11
22	20.05 ± 1.74	11.39 ± 0.82	23.63 ± 1.14	25.55 ± 1.63
23	6.31 ± 0.75	5.83 ± 0.98	1.37 ± 0.47	4.89 ± 0.37
26	0.083 ± 0.023	0.054 ± 0.090	0.045 ± 0.190	0.044 ± 0.013
27	0.094 ± 0.040	0.058 ± 0.120	0.079 ± 0.160	0.053 ± 0.050

28	0.120 ± 0.130	0.062 ± 0.080	0.087 ± 0.070	0.089 ± 0.200
29	0.006 ± 0.004	0.014 ± 0.008	0.050 ± 0.024	0.017 ± 0.005
[b]CDDP/**26**	0.076 ± 0.035	0.062 ± 0.049	0.050 ± 0.095	0.029 ± 0.010
[c]CDDP	8.22 ± 0.91	7.21 ± 0.83	5.45 ± 1.26	9.05 ± 0.55
[d]Oxa	11.95 ± 1.43	8.29 ± 0.76	12.06 ± 1.66	16.09 ± 2.44

[a]IC_{50} values were presented as means ± SD of three independent experiments; [b]CDDP/26, cisplatin/26 mixture (1:1, n/n); cisplatin; [c]CDDP, cisplatin; [d]Oxa, oxaliplatin.

In Vitro Antiproliferative Activity of 29 against CDDP/Doxorubicin-Resistant Cancer Cells and Normal Cells. Development of multidrug resistance to classical chemotherapeutic agents (e.g. cisplatin, doxorubicin) is the main reason for the fail of most first round chemotherapy. It was revealed that the overexpression of ATP binding cassette (ABC) transporters is responsible for the resistance since such transporters could enable the tumor cells to pump out drugs so that reduce the intracellular drug concentrations. According to the previous report, Rigosertib was highly active against multidrug resistant tumor cell lines that overexpressing ABC transporters [16]. This is probably because the structure of Rigosertib cannot act as the substrate for ABC transport proteins, thus cannot be moved out the cell by ABC transport. So, it will be interesting to investigate whether our target compounds which are Rigosertib derivatives could also overcome the multidrug resistance. Thus, the most active compound **29** was selected to test the cytotoxicity against CDDP resistant A549 cells (A549/CDDP), doxorubicin resistant A549 cells (A549/DOX) and CDDP resistant SKOV3 cells (SKOV3/CDDP) as well as human umbilical vein endothelial cells (HUVEC), using **26** and CDDP as controls, respectively. To verify that those multidrug-resistant cancer cell lines were successfully constructed, we firstly performed MTT assays and western blotting assays to identify whether they were drug-resistant or not. As shown in **Figure S1** and **Table S1**, the IC_{50} values of A549/CDDP, A549/DOX and SKOV3/CDDP were significantly increased when compared with those corresponding drug-sensitive A549 and SKOV-3 cancer cell lines. The resistant factors (RF) of A549/CDDP, A549/DOX and SKOV3/CDDP improved more than 4, 15 and 4 times than A549 and SKOV-3, respectively. Besides, western blotting assays also revealed that P-glycoprotein (P-gp) in A549/CDDP, A549/DOX and SKOV3/CDDP was also improved. Therefore, those drug-resistant cancer cell lines were successfully constructed. The results of **29** against the drug-resistant cancer cells were shown in **Table 2**. After 72 h co-incubation, both **26** and **29** showed high cytotoxicity to the drug

resistance tumor cells with very low IC_{50} values from 0.008 to 0.094 μM and the resistant factor no more than 1.5. In contrast, the activity of CDDP against A549/CDDP cells (IC_{50} value was 35.77 μM) and SKOV-3/CDDP cells (IC_{50} value was 28.67 μM) were significantly decreased as compared to that of non-resistant A549 and SKOV-3 tumor cells (RF values were 4.4 and 5.3, respectively) (**Table 2**). These results indicated that the A549/CDDP, A549/DOX and SKOV3/CDDP cells showed obvious resistance to cisplatin while were sensitive our designed compound **29**, meaning **29** may overcome the multidrug resistance. Furthermore, in order to compare **29** with the combination administration of **26** with cisplatin, the cytotoxicity of **26**/cisplatin mixture (1:1, n/n) was also measured. It was found that its activity was comparable to that of **26**, but lower than **29**, especially to the A549 cells. Particularly, the mixture showed highest toxicity to human normal cells (IC_{50} 0.78 μM against HUVEC cells), suggesting a serious safety risk. In contrast, compound **29** showed only moderate cytotoxicity to human normal cells (IC_{50} 8.74 μM against HUVEC cells), at least 100-fold lower than that against tumor cells, indicating a good safety and a wide therapeutic window for compound **29**.

Table 2. IC_{50} values in vitro of tested compounds in various CDDP-resistant cancer lines and human normal cells.

	[a]IC50 (μM)			
Compounds	**26**	**29**	CDDP	CDDP/**26**
A549	0.083 ± 0.023	0.006 ± 0.004	8.22 ± 0.91	0.089 ± 0.055
SKOV-3	0.045 ± 0.009	0.050 ± 0.024	5.45 ± 1.26	0.051 ± 0.020
A549/CDDP	0.094 ± 0.040	0.008 ± 0.011	35.77 ± 2.24	0.082 ±0 .035
SKOV-3/CDDP	0.041 ± 0.039	0.038 ± 0.025	28.67 ± 2.24	0.050 ± 0.030
A549/DOX	0.081 ± 0.020	0.009 ± 0.005	18.81 ± 0.95	0.076 ± 0 .039
HUVEC	3.59 ± 0.55	8.74 ± 0.44	9.03 ± 0.78	0.78 ± 0.55
[b]RF1	1.1	1.3	4.4	0.9
[c]RF2	0.9	0.8	5.3	1.0
[d]RF3	1.0	1.5	2.3	0.9

[a]IC_{50}, values were presented as means ± SD of three independent experiments; [b]RF1, Resistant Factor = IC_{50} (A549/CDDP)/IC_{50} (A549); [c]RF2, Resistant Factor = IC_{50} (SKOV-3/CDDP)/IC_{50} (SKOV-3); [d]RF3, Resistant Factor = IC_{50} (A549/DOX)/IC_{50} (A549).

HPLC Analysis on the Release of Rigosertib Moiety under the Reduction of Ascorbic Acid. The target compounds, especially compound **29**, showed remarkable activity to both normal and drug-resistant tumor cells. This exciting result might be attributed to that the Pt(IV) part of the target compound could be reduced to release the corresponding Pt(II) part and the Rigosertib moiety under reduction, thus a synergistic effect can be achieved. In order to prove this drug design strategy, HPLC analysis was performed for compound **29** which was co-cultured with/without ascorbic acid (3.0 equiv.) in a mixture of PBS (pH= 7.4) and acetonitrile (90:10, v/v) and preserved at 37 °C water bath in dark. Compound **26** and ascorbic acid dissolved in the same solvent mentioned above were used as controls to match the peaks of compound **29** in the reduction process. As shown in **Figure S2D**, compound **29** was stable in 72 h in the PBS (pH=7.4) solution. In view of the acidic microenvironment of tumor cells, the stability of **29** in the PBS (pH=5.5) was also investigated. The results in **Figure S2E** showed that more than 90 % percent of 29 remained stable in the solution within 24 h. However, when mixed with ascorbic acid, two peaks (i.e. ascorbic acid and compound **26** peaks) appeared as time passed. The peak of compound **29** gradually decreased with an increasing peak at the position of compound **26**, indicating that compound **29** could release compound **26** upon the reduction of ascorbic acid. Unsurprisingly, no peak of cisplatin was detected because of its weak chromophore under the tested condition. In all, compound **29** was stable under physiological condition and could be effectively reduced to release **26** within 5 h when exposed to ascorbic acid.

In order to verify that **29** can release **26** and CDDP in cells and detect the concentration of **26** in cancer cells, HPLC analysis was performed. Briefly, A549 cells was co-incubated with **29** (10 μM, 5 μM, 2 μM) for 24 h, washed with PBS and lysed to obtain cell lysates. Supernatant fraction gained after centrifugation was recorded and analyzed with RP-HPLC (waters, e2695 system; 2489 UV/Vis detector). The standard curve of **26** was displayed in **Figure S3** and **Table S2**, and the results of cell lysates were shown in **Figure S4** and **Table S3**. As shown in **Figure S4**, no peak of **29 (**Rt =6.8 min**)** but only **26** (Rt =8.1 min) was detected, illustrating that **29** was fully reduced to **26** in A549 cells in 24 h. The reduction of **29** in A549 cells was further proved with HR-MS in **Figure S4D** (**26**, M+H=452.1359) and **Figure S4E** (CDDP, M+Na=322.9356). As for the intracellular concentration of **26**, 0.77 μM, 2.88 μM or 5.91 μM of **26** could be detected after A549 cells co-incubated with 2 μM, 5 μM or 10 μM of **29**, respectively. Therefore, we conclude

that **29** can be fully reduced in A549 cells in 24 h to release **26** and CDDP.

Cellular Uptake. Compound **29** showed excellent cytotoxicity in the cellular assays, which may, according to the former findings, be partly attributed to the improved cellular uptake [29-33]. Therefore, to testify this hypothesis, we used ICP-MS to measure the intracellular platinum content. After 12 h co-incubation with **29** (5 μM and 10 μM) or CDDP (5 μM and 10 μM), the platinum content in A549 cells was determined by ICP-MS after digestion with 65% nitric acid. As shown in **Figure 3**, the accumulation of platinum of **29** was evidently enhanced compared with that of CDDP. Moreover, as the concentration increased, A549 cells internalized more platinum than those treated with CDDP at equal concentration (**Figure 3**). This may be associated with the hydrophobic ligands which increased the lipophilicity of the Pt(IV) complexes and contributed to the transportation trough cell membrane. The more uptake of **29** also corresponds to the increased anti-tumor activity in vitro in **Table 1**.

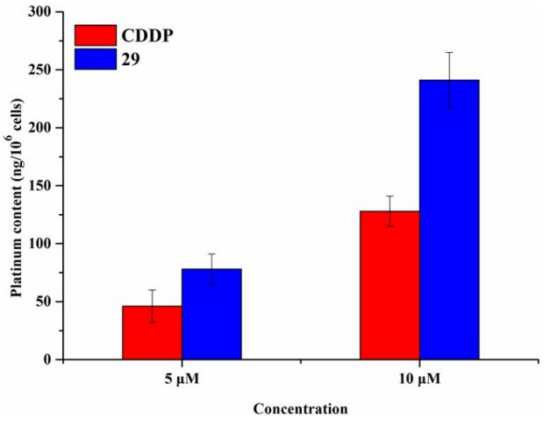

Figure 3. Cell uptake of 26 in A549 cells treated with **29** for 12 h at the concentration of 5 μM and 10 μM. Platinum content was measured by ICP-MS after digestion with 65% HNO_3. Data represented the mean ± SD of at least three different experiments.

Effect of 29 on RAS/RAF Interaction. Originally, Rigosertib was reported to be a non-ATP competitive Plk1 inhibitor in nanomole concentration [17]. However, subsequent experiments of Plk1 kinase activity test indicated that Rigosertib, **20** and **26** had little effect on kinase activity (data was not shown) [17]. Later, Reddy and co-workers reported that Rigosertib acted as RAS mimetic blocking signals that associated with downstream effector proteins [8]. Therefore, in order to determine whether our target compounds could also block the RAS/RAF/MEK/ERK signaling pathway, we conducted a series of western blot to study the effect of **26** and **29** on RAS/RAF

complex and MAPK signaling cascade. Briefly, A549 cells were co-incubated with **26** (5 μM) and **29** (5 μM) for 24 h, then the coprecipitation obtained using VE-cadherin (containing anti-RAS antibody) was further purified with protein G agarose and subjected to western blot to determine the levels of its associated CRAF. For the analysis of effects on the phosphorylation and expression of MEK and ERK, A549 cells were treated with CDDP (5μM) or different concentrations of **26** and **29** for 24 h, then the levels of phosphorylation and expression of MEK and ERK were measured, using GAPDH as loading control. As shown in **Figure 4A** and **4B**, the levels of CRAF proteins which were associated with RAS proteins were reduced in input group, whereas little effect on the expression of RAS was observed. This result suggested that **26** and **29** did disturb the interaction between RAS and CRAF, which was consistent with the result reported previously [8]. Moreover, the levels of RAS/CRAF complexes of cells treated with **26** and **29** in IP group were significantly decreased when compared to those of control group (**Figure 4A** and **4B**). Interestingly, the disruption of RAS and CRAF interaction may raise a question whether **29** directly targets either RAS protein or CRAF protein or both. We thereby carried out microscale thermophoresis (MST) assay and cellular protein thermal shift assay (CETSA) for further studies. As shown in **Figure 4C** and **4D**, **29** can directly target CRAF protein with high affinity at nanomolar concentration (affinity constant of Kd value was 149 nM), whereas the Kd value between **29** and K-RAS, N-RAS or H-RAS cannot be detected, even with the initial concentration was increased to 125 μM, indicating the poor affinity of **29** to K-RAS, N-RAS or H-RAS (results are shown in **Figure S5C-S5H**). The obvious difference of the affinity explained our design concept that as a derivative of styrylbenzylsulfones compound **29** still possessed the ability to target CRAF protein and acted as an inhibitor of the protein. Similarly, as the positive control, **26** also displayed high affinity with Kd value of 124 nM (results are shown in **Figure S5A** and **S5B**). Moreover, the results of CETSA assays (**Figure 4E-4F**) also showed that the level of CRAF remaining in the soluble fraction quickly decreased when the A549 cell lysates were heated from 47 to 67 ^{o}C. In contrast, when A549 cell lysates were treated with **26** or **29**, the melting temperature of CRAF from 51 to 67 ^{o}C significantly increased, indicating the tested compounds can effectively bind and stabilize CRAF. However, as for RAS, the melting temperature of RAS hardly changed when A549 cell lysates were treated with **26** or **29** as compared with the negative DMF treatment group (**Figure S6A** and **S6B**). Besides, the results of GAPDH in the CETSA assay

showed that both **26** and **29** had no effect on the thermal stability of GAPDH (**Figure S6C** and **S6D**). From these results, we could conclude that **29** could directly bind to CRAF protein rather than RAS protein, and disrupt the signaling transferred from RAS to CRAF.

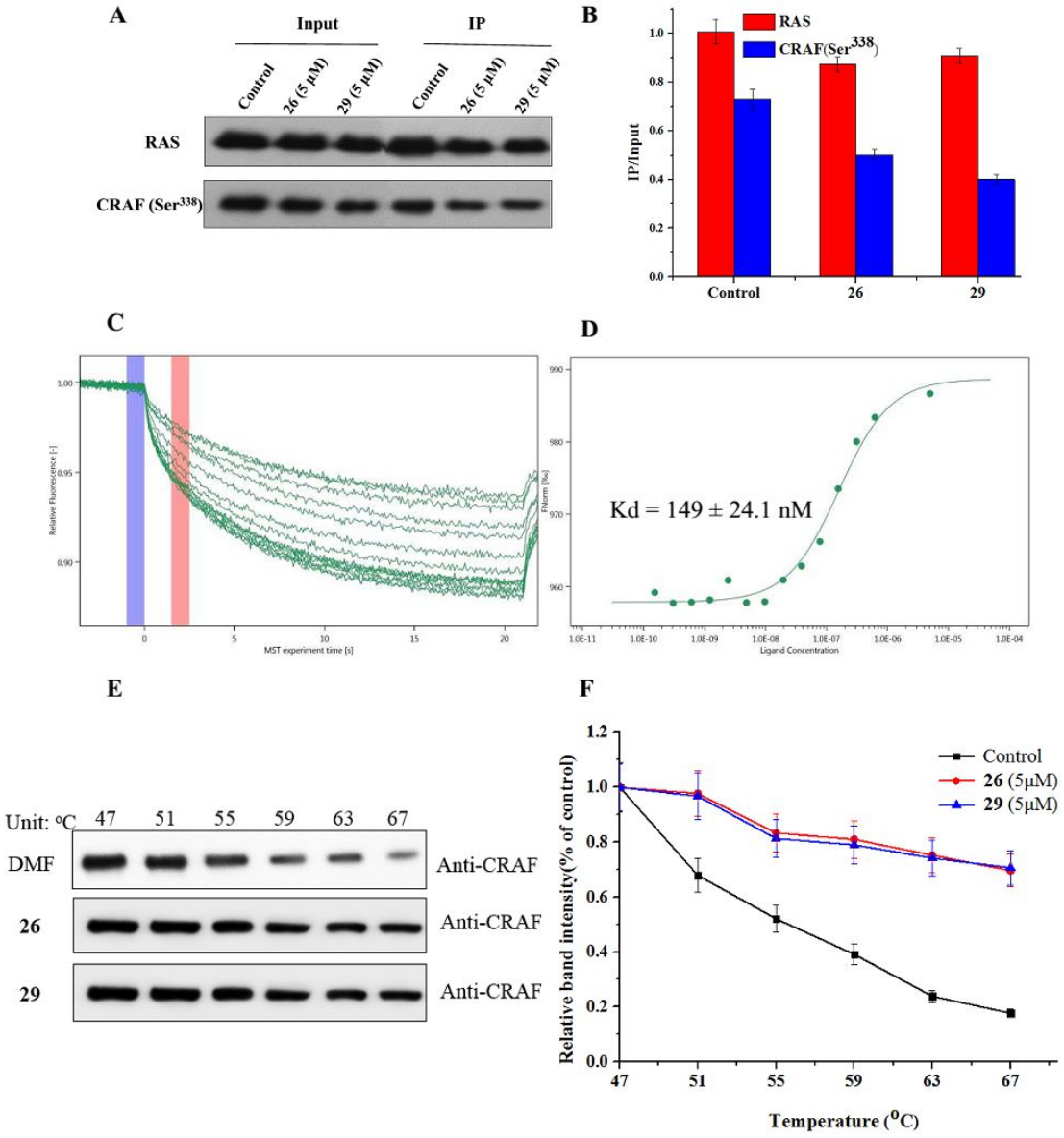

Figure 4. Compound **29** interfered with the interaction of Ras-Raf and MEK/ERK activation. (A) Cell lysates collected from A549 cells that were pretreated with **29** (5μM) and **26** (5μM) for 24 h were subjected to immunoprecipitation with anti-Ras antibodies and determined the associated CRAF with western blot. (B) Statistics of grey intensity were normalized with input. Data were presented as the mean ± SD of three independent experiments. (C): MST trace lines of **29** binding to CRAF-RBD protein. (D): MST results of **29** binding to CRAF protein. Results provided above showed that **29** binds to the CRAF protein (Kd values was 149 nM). (E) Thermal stability of RAS; (F) Statistics of grey intensity were normalized with grey intensity of 47 °C. Data were presented

as the mean ± SD of three independent experiments.

RAF kinases were essential for RAS-RAF-MEK-ERK pathway signaling. The RAF kinases can form dimers just like other protein kinases, which were RAS-dependent. Under normal signaling transduction condition, the dimers occurred in plasm and disassociated by the feedback of activation of ERK [35-37]. Thus we conducted western blotting to detect the activation of BRAF in A549 cells which were pretreated with CDDP (5 μM), **26** (2μM, 5μM) **29** (2μ, 5μM) for 24 h by using BRAF antibodies. The results in **Figure S7A** and **S7B** showed that **26** and **29** could inhibit the activation BRAF in a dose-dependent manner while **29** (2 μM) was weaker than **26** (2 μM) in this assay. Thereafter, to detect the effects of **29** on the RAS-mediated signaling, heterodimerization of endogenous CRAF and BRAF with the stimulation of EGF was investigated by co-immunoprecipitation assays, using CRAF antibodies to detected the levels of associated BRAF. The results were displayed in **Figure S7**C and **Figure S7D**, from which we could see that no BRAF protein in IP group was detected when A549 cells were treated with control (DMF without EGF), though BRAF protein existed in Input group [8]. The formation of CRAF and BRAF dimers was found upon the stimulation of EGF. However, significant decrease occurred in their dimers after 24 h co-incubation of A549 cells with **26** (5 μM) or **29** (5 μM), revealing that both **26** and **29** could also disrupt the interaction of CRAF and BRAF by interrupting the signaling between RAS and RAF. Not surprisingly, CDDP had no activity in both assays. In all, **29** could inhabit the activation of BRAF and disrupt the signaling transduction from RAS to CRAF.

As for the classical MAPK signaling cascade, the block signaling between RAS and RAF usually led to the down-regulation of phosphorylation of MEK and ERK. Indeed, the inhibition of phosphorylation were observed in our study, as shown in **Figure 5A** and **5B**. As expected, treatment with **26** or **29** resulted in reduced phospho-MEK and phospho-ERK levels in a dose-dependent manner (**Figure 5A** and **5B**). However, little effect on phosphorylation of MEK and ERK was found in CDDP-treated group, which explained indirectly that anti-tumor activity of CDDP was not involved in this signaling pathway. In summary, these findings supported our hypothesis that **29**, similar to Rigosertib, could disturb the MAPK signaling transduction by inhibiting the formation of RAS/ RAF complexes.

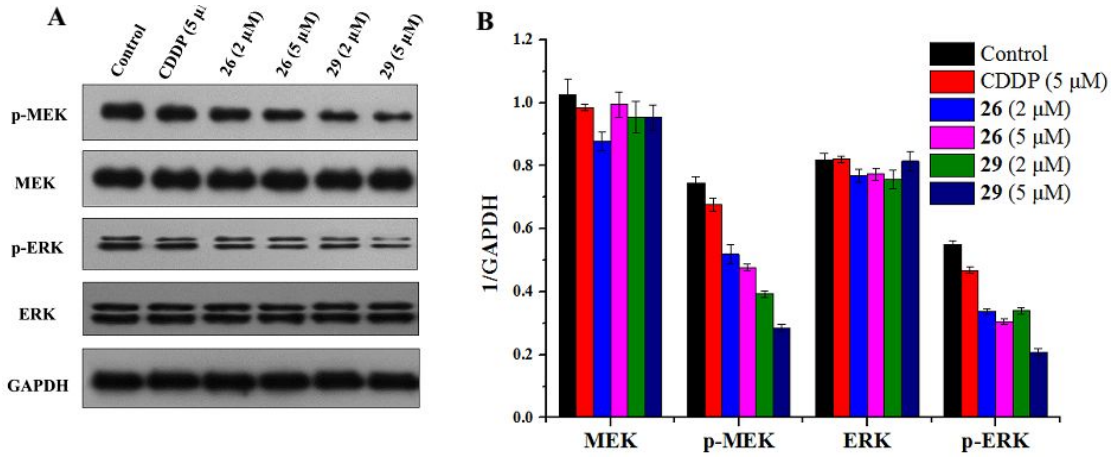

Figure 5. (A) Phosphorylation and expression of the indicated proteins determined by western blot in A549 cells after treatment with CDDP or increasing concentrations of **29** and **26**. (B) Signals obtained from western blot and normalized with GAPDH. Data were presented as the mean ± SD of three independent experiments

A549 Apoptosis Induced by 29. To further investigate whether compound **29** produced cytotoxicity by inducing apoptosis of tumor cells, cell apoptosis analysis was carried out. A549 cells were firstly treated with compound **29** (5 μM), compound **26** (5 μM) as well as CDDP (5 μM) which was used as positive control for 24 h. Thereafter, the tumor cells were co-stained with Annexin-V FITC and PI and the apoptotic cells were analyzed with flow cytometry. The result of apoptotic value was shown in **Figure 6**, from which four states of cells were found: necrotic cells (Q1), late apoptotic(Q2), early apoptotic cells (Q3) and living cells(Q4). A great difference of the apoptotic value was presented clearly. One hand, compound **29**, compound **26** and CDDP could efficiently induced apoptosis in A549 cells at the concentration of 5 μM and the apoptotic values (including the early and late apoptosis states) are 40.6 %, 37.2 %, 15.55 %, respectively. On the other hand, the apoptotic value (40.6%) of compound **29** was more supior to that of compound **26** (37.2 %), and CDDP (15.55%), which revealed that compound **29** could induce more apoptosis of A549 cells than that of compound **26** and cisplatin at the same concentration. Due to apoptosis data of A549 cells were obtained after 24 h co-incubation with high concentration of **29** (5 μM), **26** (5 μM) and CDDP (5 μM), we further investigated the apoptosis-inducing ability of **29**, **26**, and CDDP with the concentration at the IC_{50} value level and total 72 h drug exposure. From **Table S4**, we could find that **26** and **29** did not cause significant apoptosis in the first 24 h. However, when A549 were exposed to **29**, **26** and CDDP for 72 h much more cells were in apoptotic state even at the concentration of IC_{50} values (the results were shown in **Figure S8**). Altogether, **29** showed a

similar antitumor behavior by inducing apoptosis of tumor cells as compound **26** and CDDP did, but its potency was much higher than the others.

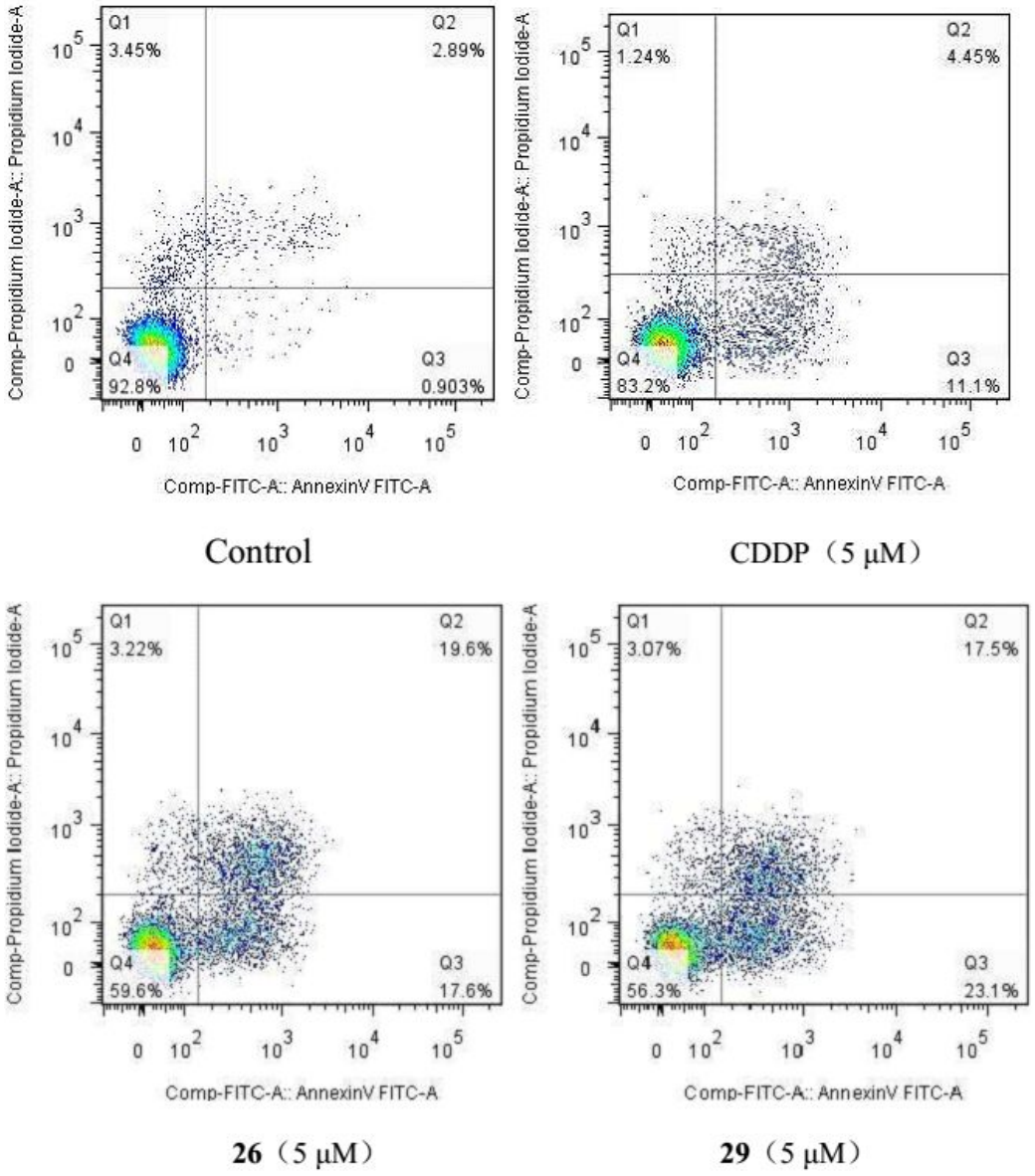

Figure 6. Annexin V-FITC and PI staining to evaluate apoptosis in A549 cells treated with various compounds. A549 cells were co-incubated with DMF, cisplatin (5 μM), compound **26** (5 μM) and compound **29** (5 μM), stained with Annexin V-FITC and PI and analyzed with flow cytometry.

Cell Cycle Arrest Analysis. It was well demonstrated that **29** and cisplatin produced cytotoxicity by inducing apoptosis. Therefore, to study the effect of the target complexes on tumor cell cycle, **26** (5 μM) and **29** (5 μM) were incubated with A549 cells overnight using CDDP (5 μM) and DMF as postive and negative control, respectively. As the results of cell arrest shown in **Figure 7**, CDDP mainly arrested A549 cells in S phase when compared to that of control group,

whose value increaed from 24.25% to 32.47%. However, the cells treated with **26** (5 μM) were mainly arrested in G2/M phase with the percentage of 68.83%, whereas the values were 12.25% and 7.72% for control and cisplatin respectively. Intrestingly, when the tumor cells were treated with the same concentration of compound **29** (5 μM), the percentage of cells arrested in G2/M phase was larger than that of compound **26** (5 μM) and control. In conclusion, compound **26** and **29** could produce cytotoxicity by introducing cell arrest in G2/M phase.

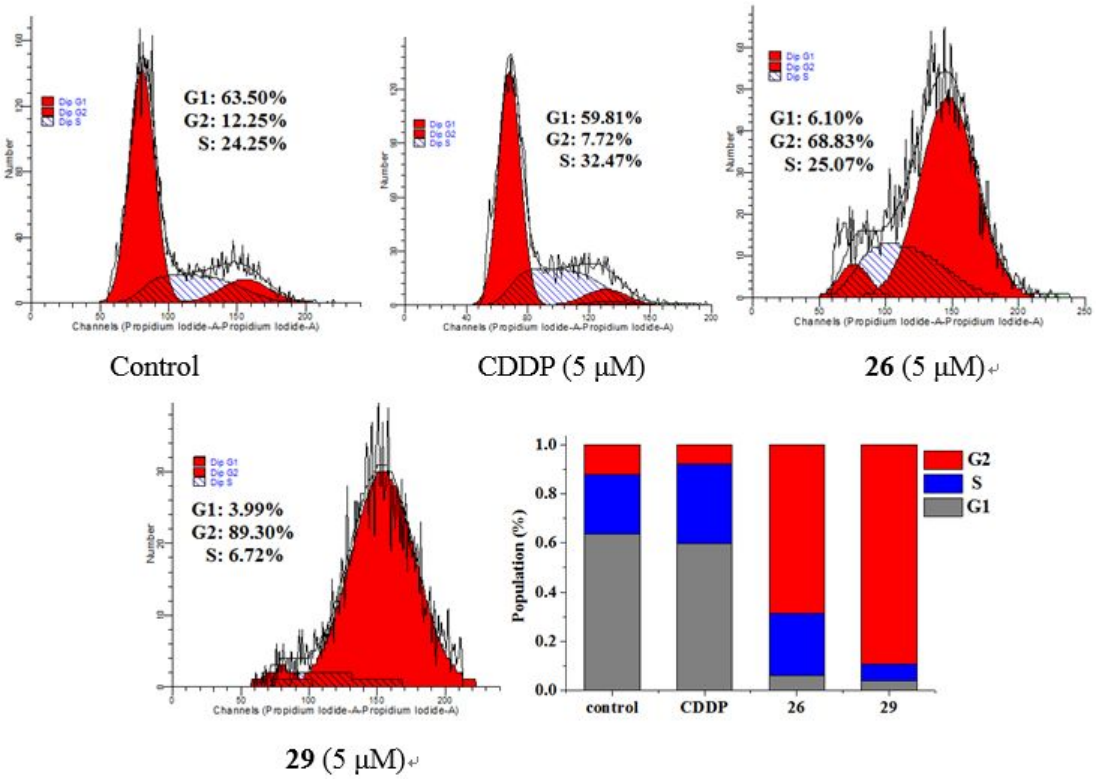

Figure 7. Cell cycle arrest was analyzed after 24 h treated with various compounds. A549 cells were treated with DMF, CDDP (5 μM), **26** (5 μM) and **29** (5 μM), stained with PI and analyzed with flow cytometry.

DNA Damage Induced by 29. It is well known that Pt(IV) complexes exsert anti-tumor activity mainly denpend on the release of Pt(II) complexes [34-37]. Previously we proved that **29** could release **26** and CDDP under the reductive condition in cells. Therefore, we performed comet assays and wetern blotting assays to verify whether **29** could also cause DNA damage. As shown in **Figure 8**, A549 cells were induced apparent DNA damage after 24 h co-incubation with CDDP (5 μM), **26** (5 μM) and **29** (5 μM), which was characterized by the tail DNA. Normally, the number and length of tail DNA were in positive correlation with the digree of DNA damage. As shown in **Figure 8** more and longer tail DNA exsited in A549 cells treated with **29**, whereas less and shorter DNA tails were found in CDDP-treated group and **26**-treated group. This indicated

that **29** induced stronger DNA damage than **26** and CDDP. Usually, the DNA damage induced by CDDP was along with double-strand break (DSB) [38-40]. Therefore we detected the expression of H2AX phosphorylation (γH2AX), a hallmark of DNA DSB. As indicated in **Figure S9A** and **S9B**, after 24h co-incubation of A549 cells with **29** (2 μM,5 μM) and CDDP (5 μM) the level of γH2AX was significantly increased when compared with control group. The **29**-treated group produced higher level of discrete γH2AX in a dose-dependent manner than CDDP-treated group, which explained that **29** increased the extent of DSB. Subsequently, the increased DSB in A549 cells also promote the expression of p53 protein, which usually occurred in an activation of the mitotic checkpoint following drug exposure [34a]. In **Figure S9A** and **S9B**, higher level of p53 was induced in A549 cells by **29** (2 μM,5 μM) than CDDP (5 μM) in a dose-dependent manner. This also incadicated that **29** can not only arrest A549 cells in G2/M phase but induced DNA damage and finally induced more apoptosis as just shown in **Figure 6** and **Figure S8**.

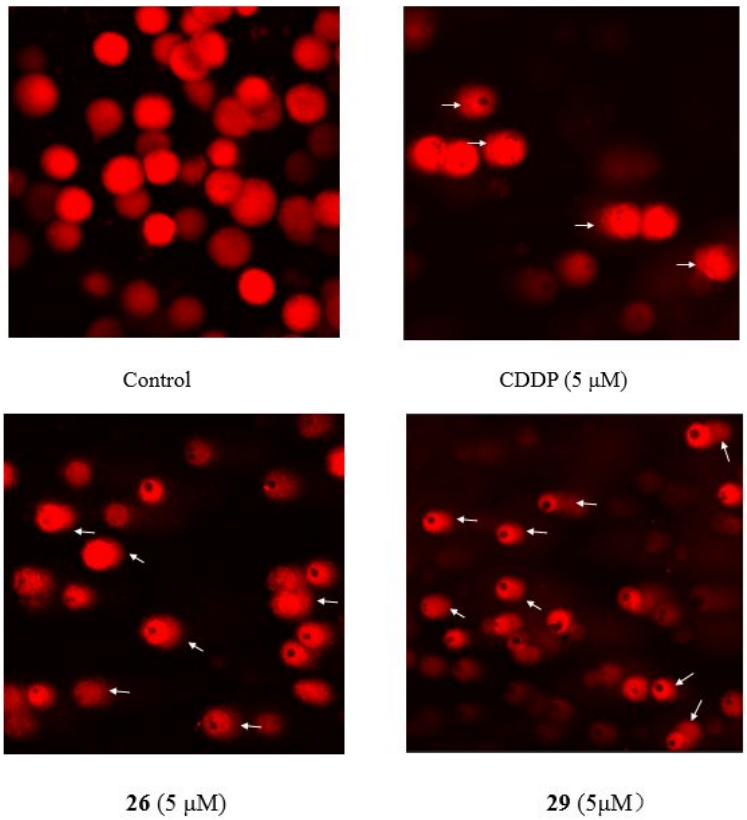

Figure 8. After 24 h treatment with vehicle, cisplatin (5 μM), **26** (5 μM) and **29** (5 μM), A549 cells were transferred onto comet slide and treated according to the method reported previously[38]. Images were analyzed and recorded with laser confocal microscope. Tail DNA was marked with white arrow.

Detection of Reactive Oxygen Species Active Oxygen. According to previous reports [32-34], metal complex broke the balance of intracellular redox to induce excess ROS accumulation.

Therefore, in order to study the accumulation of intracellular ROS, A549 cells were incubated with following compounds respectively： vehicle (DMF), CDDP (5 μM), **26** (5 μM) and **29** (5 μM). After 24h treatment, the tumor cells were stained with DCFH-DA (Molecular Probe, Beyotime, Haimen, China) and were observed and recorded with fluorescence microscope. The results were shown in **Figure 9**, from which we could see that the treatment with cisplatin significantly increased the level of intracellular ROS. Similarly, complex **26** and **29** also caused the increased level of ROS, and the fluorescence intensity of later two was higher than that of cisplatin, suggesting higher ROS levels caused by **26** and **29**. It is widely accepted that high level ROS produces high cytotoxicity. Thus, these results were consistent with former findings [34, 41a].

Generally, mitochondria are responsible for production of ATP and provide the energy using for cellular biological functions. In mitochondrial electron transport chain, only 1–2% of molecular oxygen consumed by mammalian cells turned into ROS via electron leakage [41-43]. Therefore, the endogenous ROS was mainly from mitochondria in human and animal cells. Given the significant accumulation of ROS in A549 cells displayed in **Figure 9** after co-incubation with **26**, **29** and CDDP, we observed the cellular location of ROS in A549 cells to confirm the distribution of ROS and to verify the source of ROS. The ROS was traced with DCHF-DA as green fluorescence (**Figure S10A2-D2**), while the mitochondria were highlighted by Mito Tracker RED as red fluorescence (**Figure S10A3-D3**). In **Figure S10A3**, without drug treatment, the red mitochondria were regularly distributed around the cell nucleus, and only a little green fluorescence was detected. However, much more ROS in A549 cells with green fluorescence was detected and distributed in the whole cell cytoplasm upon treated with **26**, **29** or **CDDP** with the same concentration. However, the merging images in **Figure S10A4-D4** displayed that the location of ROS and mitochondria did not overlap well. The Pearson's R value analyzed according to the 2D intensity histogram by ImageJ lab program was shown in **Figure S10A4-1** to **D4-1**, from which we could see that ROS was irrelevant to mitochondria. Thus, the results suggested that the production of ROS may not come from mitochondria itself.

To confirm whether intrinsic luminescence of compounds that would interfere with the results of the luminescence of ROS tracker, we next tested the fluorescence emission spectra of **26**, **29** in various solutions (λ_{ex} = 315 nm， λ_{ex} = 494 nm, λ_{ex} = 535 nm). Not surprisingly, negligible fluorescence emission spectra were obtained (**Figure S11**).

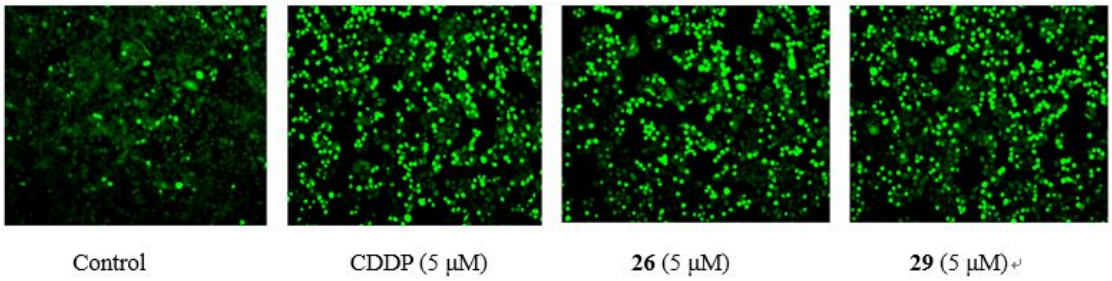

Figure 9. After 24 h treatment with vehicle, cisplatin (5 μM), **26** (5 μM) and **29** (5 μM), A549 cells were incubated with fluoresce probe DCFH-DA. Images were analyzed and recorded with fluorescence microscope.

The Decreasing of Mitochondrial Membrane Potential Induced by 29. As we have found that **26** and **29** could induce the accumulation of ROS in cells, it will be interesting to investigate whether the enhanced formation of ROS in cells could make the decrease of mitochondrial membrane potential (MMP) [41a, 44,45], which was the notable hallmark of classical mitochondrial apoptosis pathway. Therefore, A549 cells were incubated with **26** (5 μM), **29** (5 μM) or CDDP (5 μM), using equal DMF as negative control. After 24 h treatment, cells were stained with JC-1 test kit , analysed and recorded with flow cytometry. The result of MMP was shown in **Figure 10**, from which we could see that the $\Delta\Psi$m of cells treated with three compounds mentioned above was decreased relative to control, indicating the damage of the cells which eventually resulting in apoptosis.

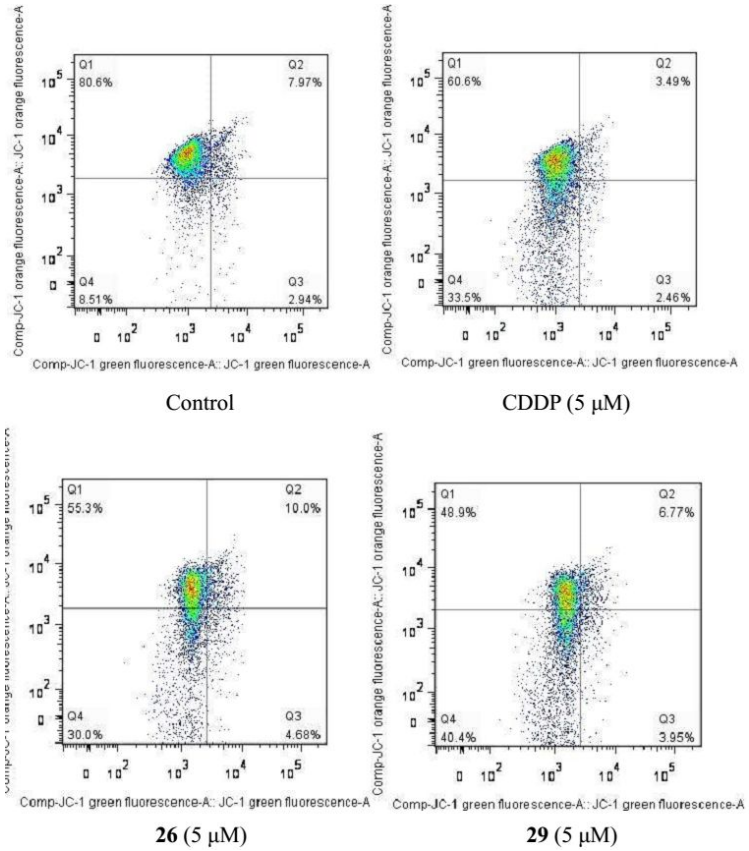

Figure 10. After 24 h treatment with vehicle, CDDP (5 μM), **26** (5 μM) and **29** (5 μM), A549 cells were stained with JC-1 probe. Mitochondrial membrane potential ($\Delta\psi_m$) were analyzed and recorded with flow cytometry.

Cell Morphology of Apoptosis Induced by 29. In order to investigate cell morphology of apoptosis, A549 tumor cells were treated with various compounds: **26** (5 μM), **29** (5 μM), CDDP (5 μM), and vehicle (DMF) for 24 h. Then the cells were co-stained with AO (6 μg/mL) and EB (6 μg/mL) and apoptotic morphology was analyzed with fluorescence microscope. The result was shown in **Figure 11**, from which different nuclear morphology could be found. The cells with different treatment was colored in green or orange, especially for that of cisplatin, **26** and **29** groups, whose brightness was enhanced, indicating the happening of apoptosis induced by these three compounds. In addition, the tumor cells treated with **26** or **29** showed clear apoptotic state with decreased cell density, reduced cell volume and concentrated cytoplasm, which was consistent with that of cells treated with cisplatin at the same concentration. So, compound **29** could induce apoptosis just as **26** and CDDP did.

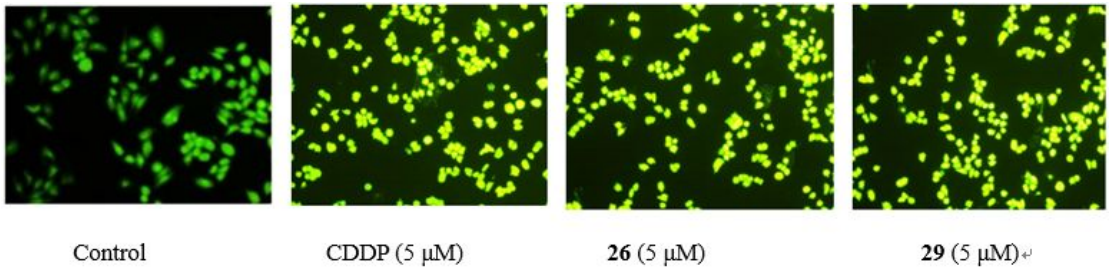

Figure 11. Morphological changes of A549 cells induces by **29**. After 24 h treatment with DMF, CDDP (5 μM), **26** (5 μM) and **29** (5 μM), A549 cells were stained with AO/EB. Results were anylyzed and recorded with a Nikon Te2000 deconvolution microscope (magnification 200×).

26 and 29 Regulated Apoptotic Related Proteins. To elucidate the mechanisms involved in potent apoptotic pathway induced by **26** (2 μM, 5 μM), **29** (2 μM, 5 μM) and CDDP (5 μM) several apoptotic related proteins, including pro- or/and anti-apoptotic proteins, such as Bax and Bcl-2 were analyzed with western blot assay. The results were shown in **Figure 12A** and **12B**. Treatment with **29** (5 μM) for 24 h induced down-regulation of anti-apoptotic protein Bcl-2 and up-regulation of pro-apoptotic protein Bax in A549 cells, which deeply caused the decrease of MMP studied above. Then the colapsed MMP actived the release of Cyt c and susequently led to the activation of downstream caspase cascade. As was shown in **Figure 12A** and **12B**, A549 cells exposed to **29** showed statistically up-regulated level of cleaved-casepase 9 and cleaved-caspase 3 along with the down-regulated level of pro-caspase 9 and pro-caspase3, which aslo contributed to the up-regulation of cleaved-parp level. It is noted that this protein-regulating activity of **29** was in a dose-dependent manner. Not surprisingly, simialr effects were aslo observed when A549 cells were treated with **26**. Besides, as the positive control, CDDP (5 μM) also showed the same activity to regulate the expression of the tested proteins, however, its potency was not comparable to that of **26** or **29** at the concentration of 2 μM or 5 μM.

Since Prolyl-isomerase 1 (Pin1), overexpressed in many cancers such as prostate, breast, and lung cancers, can also regulate the process of apoptosis [20], we detected the expression of Pin 1 in A549 cells after 24 h treatment of **26** (2 μM), **26** (5 μM), **29** (2 μM), **29** (5 μM) and CDDP (5 μM). As shown in **Figure S12**, the level of Pin 1 changed little when A549 cells were treated with tested compounds, except for the treatment of higher concentration of **29** which caused moderate down-regulation of Pin 1. The weak effect of the tested compounds on Pin 1 may be attributed to the lack of effective binding domain in Pin 1. Thus, the obtained results clearly illustrated that **29**

could effectively bind to CRAF and disrupt the signaling transduction between RAS and CRAF other than other protein, such as Pin1 -mediated pathway.

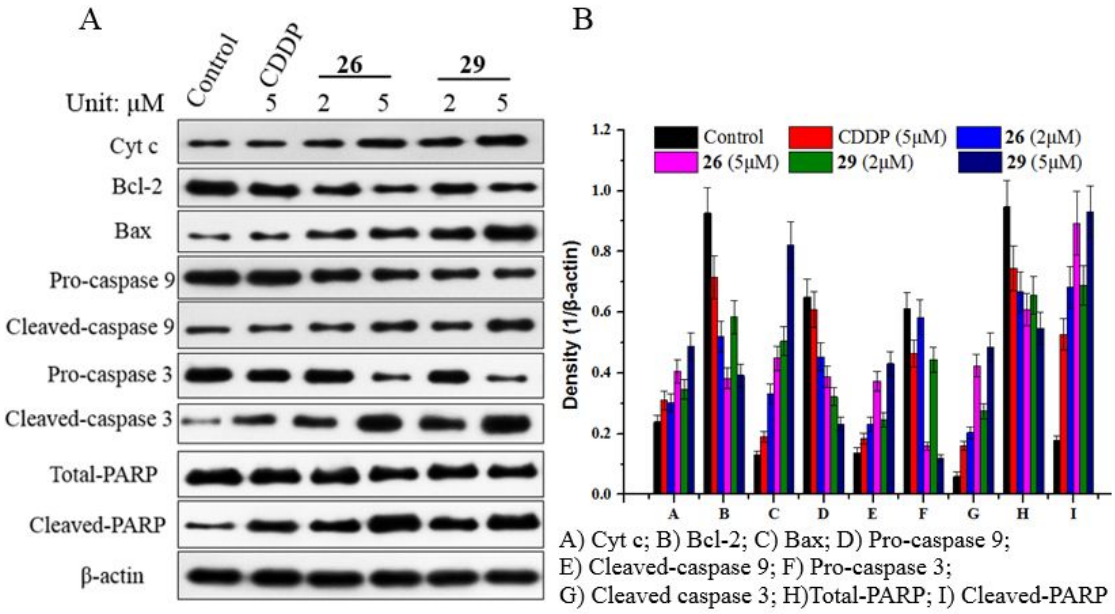

Figure 12. After 24h treatment of A549 cells with **26** (5 μM) and **29** (5 μM), (A) Western blot analysis of Cyt c, Bcl-2, Bax, Pro-caspase 9, caspase-9, Pro-caspase 3, caspase-3, Total-PARP and cleaved PARP were analyzed, using β-actin antibody was used as reference control. (B) Expression levels of (A) shown as percentages.

In Vivo Evaluation of 29 on A549 Xenograft Models. On the basis of its superior in vitro antitumor activities, **29** was selected for an in vivo xenograft mouse study. A549 cells (3×106 in 100 μL) were injected subcutaneously into the flank of the nude mice to establish tumor xenograft models. Once the tumors reached to 150-250 mm^3, those mice were divided randomly into four different groups (three mice per group) and treated via injecting intravenously following: (1) **29** (6 μmol/kg, on days 0, 2 and 4), Rigosertib (6 μmol/kg, on days 0, 2 and 4), CDDP (6 μmol/kg, on days 0, 2 and 4) and vehicle (equivalent volume of normal saline injection, on days 0, 2 and 4). As shown in **Figure 13**, compound **29** caused statistically significant inhibition of tumor growth with 52.1% (percentage of inhibition ration [IR] value, **Table S5**) as compared with that of untreated control. In addition, compound **29** (IR, 52.1%) showed better potential antitumor activity than that of positive drug CDDP (IR, 36.7%) and Rigosertib (IR, 38.0%) at equal molecular dose. The curves of **Figure 13A** and **13B** showed the same trendance. It should be noted that though Rigosertib showed strong antitumor activity at nanomolar concentrations in vitro, it only exhibited moderate tumor growth inhibition in vivo. This may be due to the low dosage used in the study [16,

[34]. Importantly, no evident side effects such as body weight loss or animal death were observed in groups treated with compound **29** and Rigosertib, as shown in **Figure 13C**. On the contrary, the CDDP-treated group showed serious toxicity as reflected by the big body weight loss, especially during the days of 6-12 after intravenous injection of CDDP. These results showed that compound **29** was efficacious against A549 tumor xenografts with good safety.

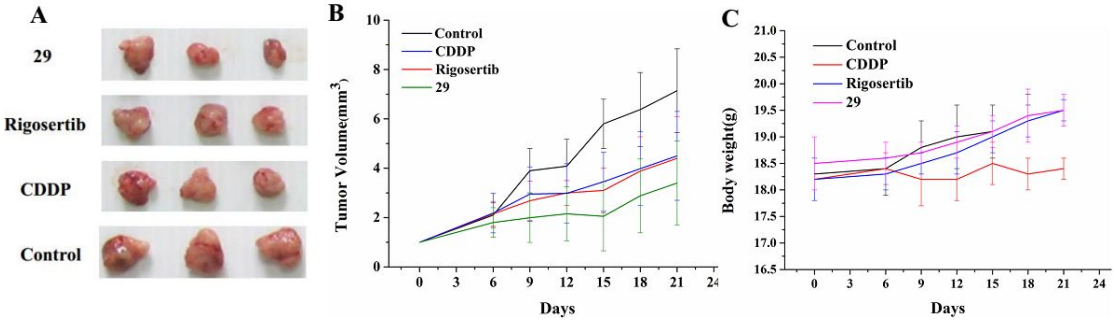

Figure 13. Antitumor activity of compound **29** on A549 xenograft models. Nude mice implanted with A549 cells in the flank were dosed via injecting intravenously of **29** (6 μmol/kg), Rigosertib (6 μmol/kg), CDDP (6 μmol/kg), vehicle (equivalent volume of normal saline injection) on days 0, 2 and 4. The mice were sacrificed and made mathematical statistics. (A) Tumor pictures obtained after sacrifice of the mice treated with **29**, Rigosertib, CDDP and vehicle. (B) The RTV (relative tumor volume) (± SEM) is graphed with error bars representing the standard deviation. (c) The average body weights (± SEM) were plotted after sacrifice of the mice treated with **29**, Rigosertib, CDDP and vehicle.

CONCLUSION

Nine styrylbenzylsulfone derivatives generated from the platinum-based modification of the side chain of Rigosertib were designed, synthesized, and tested for their biological activity. The results of MTT activity test in vitro showed that all of the synthesized target compounds showed good anti-proliferative activity against the tested cancer cells; among them compound **29** was most active with the potency higher than the positive control cisplatin and Rigosertib. Significantly, compound **29** could also inhibit the multidrug resistant tumor cells at nanomolar concentration. This unique merit of **29** may be attributed to the enhancement of cellular uptake as well as its multifunctional antitumor mechanism. As our studies revealed that **29** could effectively release Rigosertib and the corresponding Pt(II) moiety upon the reducing substances, thus the active components could exert the antitumor effect via different pathways. Indeed, we have found that **29** could, on the one hand, disturb signaling transduction between RAS and CRAF via

directly binding to CRAF protein, and finally induce downregulation of phosphor-MEK and phosphor-ERK; On the other hand, **29** could also induce apoptosis and clearly arrest the A549 cells at the G2/M phase. Furthermore, the study of apoptotic pathway showed that massive reactive oxygen species was produced when the cancer cell was treated with **29**. All of these performances of **29** are quite similar to that of platinum-based agents, suggesting that **29** maintained the cisplatin-like activity. Thus, we can summarize that **29** could inhibit the proliferation of tumor cells via two different pathways: the RAF-MEK-ERK pathway and the platinum-based cytotoxicity pathway, as outlined in **Figure 14**. Due to this multifunctional character, **29** could efficiently inhibit tumor growth in A549 xenograft model, and no obvious side effects were observed during the test. In all, these excellent performances in the pharmacological tests both in vitro and in vivo made compound **29** possible for 'efficient and hypotoxic' antineoplastic candidate.

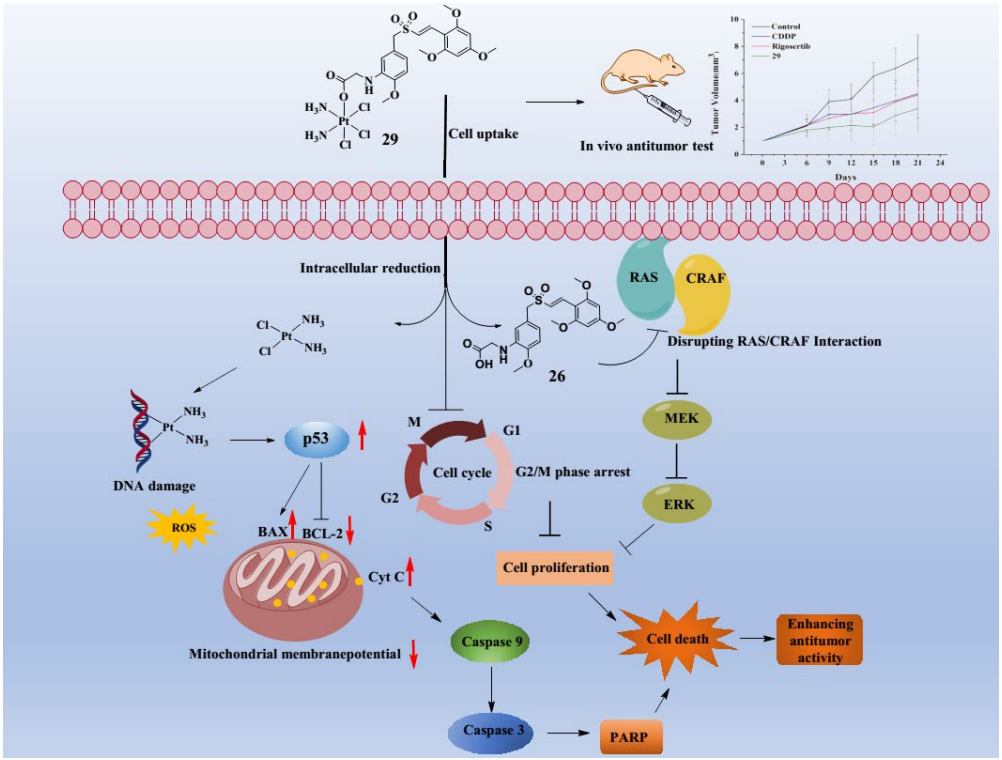

Figure 14. The proposed antitumor action mode of **29**.

EXPERIMENTAL SECTION.

(1) Materials and Instruments. All chemical reagents and solvents were purchased commercially from Aladdin, Energy Chemical or Adamas-beta and used without further purification. Potassium tetrachloroplatinate(II) was purchased from commercial sources (Lingfeng

Chemical Ltd.). ^{1}H and ^{13}C NMR spectra were obtained from with Bruker 300, 400 or 600 MHz spectrometer in DMSO-*d*6 or $CDCl_3$ and tetramethylsilane (TMS) was used as reference. Mass spectra were measured by an Agilent 6224 ESI/TOF MS instrument. All of the compounds submitted for biological studies were at least 95% purity by RP-HPLC on ODS column (250×4.6 mm, 5 μm) with an eluent of acetonitrile/water (45:55, V/V) (0.1% trifluoroacetic acid in water). Besides all cells used in this article were obtained from KeyGEN BioTECH Corp. Besides, Mitochondrion Red (KGMP0071) and ROS tracker were obtained from KeyGEN BioTECH Corp. Bax, Bcl-2, Cytochrome c, Pro-caspase-3/9, Cleaved-casepase-3/9, Total-PARP and Cleaved-PARP antibodies were purchased from Imgenex, USA. Antibodies directed against p-MEK, MEK, p-ERK, ERK, Pin 1 (#3722), p53 were purchased from Cell Signaling Technology. CRAF antibody was purchased from Affinity Biosciences, whereas RAS antibody, BRAF antibody (ab124794) was from Abcam. Secondary antibody (1:2000) labeled with horseradish peroxidase was came from Santa Cruz Biotechnologies

(2) Synthesis and Characterization of Intermediates.

Compound **1**. To a solution of compound $\mathbf{SM_1}$ (3.01 g, 18.01 mmol) and anhydrous K_2CO_3 (6.22 g, 45.03 mmol) in DMF (30 mL) was added CH_3I (3.83 g, 27.02 mmol) at room temperature and stirred overnight at the same temperature. Progress of the reaction was monitored with TLC. After completion of the reaction, solvent was evaporated under reduced pressure to obtain crude yellow solid. After that, DCM (300 mL) was added to dissolve the residue and washed with NaOH solution (1N), sat. NaCl (100 mL) . The organic layer was dried with anhydrous Na_2SO_4 and concentrated in vacuum to give pale white solid 3.05 g. Yield: 93.7%. ^{1}H NMR (500 MHz, $CDCl_3$) δ 9.94 (s, 1H), 8.34 (d, *J* = 2.0 Hz, 1H), 8.09 (dd, *J* = 8.7, 2.0 Hz, 1H), 7.25 (d, *J* = 8.7 Hz, 1H), 4.07 (s, 3H).

Compound **2**. To a solution of compound **1** (1.01 g, 5.58 mmol) in MeOH (20 ml) at 0 °C was added $NaBH_4$ (0.27g, 7.25 mmol) gradually and stirred at the same temperature for 20 min. Progress of the reaction was monitored with TLC. The reaction was worked up by quenched with HCl solution (1 N) at 0 °C and removed the solvent to obtain white solid under reduced pressure. After that, DCM (300 ml) was added to dissolve the residue, washed with sat. NaCl (3×100 mL). The combined organic layer was dried with anhydrous Na_2SO_4 and concentrated in vacuum to give white solid 1.02 g. Yield: 100%. ^{1}H NMR (500 MHz, $CDCl_3$) δ 7.83 (d, *J* = 2.1 Hz, 1H), 7.54

(dd, J = 8.6, 2.1 Hz, 1H), 7.07 (d, J = 8.6 Hz, 1H), 4.68 (s, 2H), 3.96 (s, 3H), 2.06 (s, 1H).

Compound **3**. To a solution of compound **2** (0.50 g, 2.73 mmol) in DCM (15 mL) at 0 °C was added PBr_3 (1.10 g, 4.10 mmol) gradually and stirred at the same temperature for 2 h. The reaction was monitored with TLC and quenched with $NaHCO_3$ (1 M) solution at 0 °C. After that, DCM (300 mL) was added to dissolve the residue, washed with sat. NaCl (3×100 mL). The organic layer was dried with anhydrous Na_2SO_4 and concentrated in vacuum to give white solid 0.67 g. Yield: 99.7%. ^{1}H NMR (500 MHz, $CDCl_3$) δ 7.88 (d, J = 2.2 Hz, 1H), 7.57 (dd, J = 8.7, 2.2 Hz, 1H), 7.07 (d, J = 8.7 Hz, 1H), 4.46 (s, 2H), 3.97 (s, 3H).

Compound **4**. To a solution of NaOH (162.4 mg, 4.06 mmol) in MeOH (15 mL) at 0 °C was added TGA (224.6 mg, 2.43 mmol) gradually and stirred at the same temperature for 10 min. Then compound **3** (0.50 g, 2.03 mmol) in 10 MeOH (10 mL) was dropped slowly into the solution. The reaction was monitored with TLC. After completion of the reaction, the solvent was removed under reduced pressure to obtain pale yellow solid. After that, water (50 mL) was added to dissolve the residue and adjusted the PH to 4-5 with HCl (1N) solution. The precipitate was filtered to obtain pale yellow solid 469.8 mg. Yield: 90.0%. ^{1}H NMR (500 MHz, DMSO-d_6) δ 12.53 (s, 1H), 7.82 (d, J = 2.1 Hz, 1H), 7.60 (dd, J = 8.6, 2.1 Hz, 1H), 7.32 (d, J = 8.6 Hz, 1H), 3.91 (s, 3H), 3.83 (s, 2H), 3.14 (s, 2H). HR-MS (*m/z*) (ESI): calcd for $C_{10}H_{11}NO_5S$ [M-H]: 256.0358; Found: 256.0359.

Compound **5**. To a solution of compound **4** (257.3 mg, 1.94 mmol) in AcOH (15 mL) at room temperature was added H_2O_2 (661.0 mg, 19.40 mmol) and stirred at the 50 ℃ for 3h. The reaction was monitored with TLC. After the completion of the reaction, the solvent was removed under reduced pressure to attain crude product. The residue was further purified with silica gel chromatography with the eluent of DCM and MeOH (100:0-30:1) to give pale yellow solid 413.0 mg. Yield: 73.7%. ^{1}H NMR (500 MHz, DMSO) δ 13.48 (s, 1H), 7.92 (d, J = 2.1 Hz, 1H), 7.68 (dd, J = 8.7, 2.1 Hz, 1H), 7.43 (d, J = 8.7 Hz, 1H), 4.68 (s, 2H), 4.20 (s, 2H), 3.95 (s, 3H). HR-MS (*m/z*) (ESI): calcd for $C_{10}H_{11}NO_5S$ [M-H]: 288.0250; Found 288.0254.

Compound **7**. To a solution of compound **5** (3.0 g, 10.37 mmol) in toluene (30 mL) at 40 ℃ was added piperidine (823.8 μL, 8.30 mmol) and stirred at the same temperature for 10 min. Then benzoic acid (1.3 g, 10.37 mmol) and compound **6** (2.2 g, 11.42 mmol) were added to the solution and heated to reflux overnight. Progress of reaction was monitored with TLC. After the

completion of the reaction, the solution was cooled to room temperature and filter to obtain yellow crude product. The precipitate was recrystallized with MeOH (20 mL) to get yellow solid 1.5 g. Yield: 34.1%.^{1}H NMR (300 MHz, DMSO) δ 7.88 (s, 1H), 7.64 (d, *J* = 8.6 Hz, 1H), 7.51 (d, *J* = 15.6 Hz, 1H), 7.38 (d, *J* = 8.6 Hz, 1H), 7.09 (d, *J* = 15.6 Hz, 1H), 6.29 (s, 2H), 4.54 (s, 2H), 3.93 (s, 3H), 3.85 (s, 9H).

Compound **8**. To a solution of compound **7** (1.80 g, 4.25 mmol) in EtOH (20 mL) was added H_2O (5.0 mL), NH_4Cl (136.4 mg, 2.55 mmol), Fe（1.43g，25.50 mmol）and heated to 70 °C for 4 h. Progress of reaction was monitored with TLC. After the completion of the reaction, the insoluble content was removed by filtration. Solvent of the reaction was finally evaporated under reduced pressure to give yellow solid 1.5 g. Yield: 88.2%. ^{1}H NMR (300 MHz, $CDCl_3$) δ 7.59 (d, *J* = 15.6 Hz, 1H), 7.08 (d, *J* = 15.6 Hz, 1H), 6.75 (d, *J* = 8.1 Hz, 1H), 6.64 (s, 1H), 6.50 (d, *J* = 8.1 Hz, 1H), 6.29 (s, 2H), 4.76 (s, 2H), 4.20 (s, 2H), 3.85 (s, 9H), 3.75 (s, 3H). HR-MS (*m/z*) (ESI): calcd for $C_{19}H_{23}NO_6S$ [M+H]: 394.1246; Found 394.1230.

Compound **11**. (1) To a solution of compound **9** (612.9 mg, 4.21 mmol) in anhydrous DCM (10 mL) was added oxalyl chloride (1.8 mL) at 0 °C and stirred at room temperature overnight. After completion of the reaction, the solvent was removed under reduced pressure to obtain colorless oil. The crude product was used for next step without further treatment. (2) To a solution of compound **8** (1.50 g, 3.83 mmol) in anhydrous DCM (15 mL) at 0 °C was added the compound got previously in DCM (5 mL) at the same temperature and stirred at room temperature for 10 min. After that, Et_3N (507.8 mg, 699 μL,) in DCM (5 mL) was added to the solution and stirred for another 2 h. After completion of the reaction, the residue was dissolved in DCM (300 ml) and washed with water (100 mL), sat. NaCl (3×100 mL). The organic layer was dried with anhydrous Na_2SO_4 and concentrated under reduced pressure. The crude product was further purified with silica gel chromatography with the eluent of DCM and PE (2:1) to get pale yellow solid (1.62 g). Yield: 85.0%. ^{1}H NMR (300 MHz, DMSO-d_6) δ 9.04 (s, 1H), 7.98 (s, 1H), 7.59 (d, J = 15.7 Hz, 1H), 7.11 (d, J = 15.7 Hz, 1H), 7.04 (s, 1H), 7.01 (d, J = 8.4 Hz, 1H), 6.29 (s, 2H), 4.35 (s, 2H), 3.86 (s, 9H), 3.83 (s, 3H), 3.60 (s, 3H), 2.46 – 2.29 (m, 4H), 1.86-1.76 (m, 2H). HR-MS (*m/z*) (ESI): calcd for $C_{25}H_{31}NO_9S$ [M+H]: 522.1792; Found 522.1721.

Compound **12**. Compound **8** (751.0 mg, 1.91 mmol), compound **10** (160.2 mg, 2.10 mmol), oxalyl chloride (1.0 mL), Et_3N (249.5 mg, 344 μL) and DCM 25 mL were used following the

procedure described for synthesis of compound **11**, and attained pale yellow solid (0.85 g). Yield: 84.9%. ^{1}H NMR (400 MHz, $CDCl_3$) δ 8.37 (s, 1H), 7.84 (d, *J* = 15.6 Hz, 1H), 7.72 (s, 1H), 7.15 (dd, *J* = 8.4, 2.0 Hz, 1H), 7.11 (d, *J* = 15.6 Hz, 1H), 6.87 (d, *J* = 8.4 Hz, 1H), 6.08 (s, 2H), 4.21 (s, 2H), 3.88 (s, 3H), 3.84-3.83 (m, 9H), 3.67 (s, 3H), 2.40 - 2.35 (m, 4H), 1.74 - 1.69 (m, 4H). HR-MS (*m/z*) (ESI): calcd for $C_{26}H_{33}NO_9S$ [M+H]: 536.1954; Found 536.1902.

Compound **13**. To a solution of compound **10** (1.2 g, 2.30 mmol) in EtOH (10 mL) and pure water (5 mL) was added LiOH•H_2O (243.6 mg, 5.75 mmol) at room temperature and stirred at room temperature overnight. Progress of the reaction was monitored by TLC. After the completion of reaction, the solvent was removed under reduced pressure to obtain pale yellow solid. The residue was dissolved with 30 mL pure water and adjusted the PH of the solution to 5 with HCl solution (1N), then filtered to give pale yellow solid (1.0 g). Yield: 91.0%. ^{1}H NMR (500 MHz, DMSO-d_6) δ 9.02 (s, 1H), 7.98 (s, 1H), 7.59 (d, *J* = 15.7 Hz, 1H), 7.10 (d, *J* = 15.7 Hz, 1H), 7.05 (d, *J* = 8.2 Hz, 1H), 7.01 (d, *J* = 8.2 Hz, 1H), 6.29 (s, 2H), 4.34 (s, 2H), 3.85 (s, 9H), 3.82 (s, 3H), 2.43-2.37 (m, 2H), 2.27-2.25 (m, 2H), 1.79-1.76 (m,2H). HR-MS (*m/z*) (ESI): calcd for $C_{24}H_{29}NO_9S$ [M+H]: 508.1436; Found 508.1460.

Compound **14**. Compound **12** (850.0 mg, 1.58 mmol), LiOH•H_2O (166.6 mg, 3.97 mmol), EtOH (10 mL) and pure water (5 mL) were used following the procedure described for synthesis of compound **11**, and got pale yellow solid 746.5 g. Yield: 90.0%. ^{1}H NMR (300 MHz, DMSO-d_6) δ 11.98 (s, 1H), 9.03 (s, 1H), 7.99 (s, 1H), 7.59 (d, *J* = 15.7 Hz, 1H), 7.11 (d, *J* = 15.7 Hz, 1H), 7.05 (d, *J* = 8.5 Hz, 1H), 7.01 (d, *J* = 8.5 Hz, 1H), 6.30 (s, 2H), 4.34 (s, 2H), 3.86 (s, 9H), 3.83 (s, 3H), 2.43-2.33 (m, 2H), 2.26-2.22 (m, 2H), 1.60-1.49 (m, 4H). HR-MS (*m/z*) (ESI): calcd for $C_{25}H_{31}NO_9S$, [M-H]: 520.1647; Found 520.1751.

(3) General Procedures for Preparing Compounds 18-23.

To a solution of compound **13** or **14** (0.33 mmol) in DMF (3 ml) was added compound TBTU (0.50 mmol) and stirred at room temperature for 5 min. Then, Et_3N (68.0 ul, 0.50 mmol) was added to the solution under the protection of nitrogen and stirred for 5min at the same temperature. After that, compound **15, 16** or **17**(0.36 mmol) was added to the solution under the protection of nitrogen and stirred for 2 h at 35 ℃. Progress of the reaction was monitored with TLC. After the completion of the reaction, DCM (250 mL) was added to the solution and washed with sat. NaCl (150 mL). The organic layer was dried with anhydrous Na_2SO_4 and concentrated

under reduced pressure to obtain crude product. The crude product was further purified with silica gel chromatography with the eluent of DCM and MeOH (60:1-20:1) to give target product.

Compound **18**. Yield: 36.2%.^{1}H NMR (300 MHz, DMSO-d_6) δ 9.58 (s, 1H), 8.94 (s, 1H), 8.13 (s, 1H), 8.02 (s, 1H), 7.78 (s, 1H), 7.59 (d, J = 15.6 Hz, 1H), 7.41 (s, 1H), 7.10 (d, J = 15.6 Hz, 1H), 7.03-6.99 (m, 2H), 6.29 (s, 2H), 4.34 (s, 2H), 3.85 (s, 9H), 3.82 (s, 3H), 2.83-2.71 (m, 2H), 2.44 – 2.39 (m, 2H), 2.32 – 2.28 (m, 2H), 2.21 – 2.16 (m, 1H), 2.08 – 2.04 (m, 1H), 1.81 – 1.76 (m, 2H), 1.56-1.49 (m, 3H), 1.33-1.25 (m, 1H), 1.11-1.03 (m, 2H).^{13}C NMR (75 MHz, DMSO-d_6) δ 183.39, 171.29, 163.99, 160.89 (C×2), 149.89, 133.37, 127.68, 127.50, 124.82, 123.98, 120.88, 111.02, 102.88, 91.40 (C×2), 63.71, 62.91, 60.06, 56.55 (C×2), 56.23, 56.12, 37.12, 35.82, 31.36, 31.30, 24.16 (C×2), 22.28. HR-MS (*m/z*) (ESI): calcd for $C_{30}H_{42}Cl_3N_3O_9PtS$, [M-H]: 920.1480; Found 920.1414.

Compound **19**. Yield: 33.6%.^{1}H NMR (300 MHz, DMSO-d_6) δ 9.61 (s, 1H), 8.99 (s, 1H), 8.12 (s, 1H), 8.00 (s, 1H), 7.77 (s, 1H), 7.59 (d, J = 15.5 Hz, 1H), 7.41 (s, 1H), 7.11 (d, J = 15.5 Hz, 1H), 7.02 (s, 2H), 6.30 (s, 2H), 4.34 (s, 2H), 3.85 (s, 9H), 3.83 (s, 3H), 2.39-2.35 (m, 2H), 2.30-2.25 (m, 2H), 2.21-2.02 (m, 3H), 1.55-1.48 (m, 7H), 1.30-1.24 (m, 1H), 1.16 – 0.96 (m, 3H). ^{13}C NMR (75 MHz, DMSO-d_6) δ 183.57, 171.94, 164.28, 161.31（C×2), 149.97, 133.34, 127.70, 127.45, 124.91, 124.04, 121.09, 111.17, 103.05, 91.41 (C×2), 63.91, 62.62, 60.35, 56.55 (C×2), 56.23, 56.12, 37.43, 36.18, 31.37, 31.29, 25.53 (C×2), 25.15, 24.00. HR-MS (*m/z*) (ESI): calcd for $C_{31}H_{44}Cl_3N_3O_9PtS$, [M-H]: 934.1282; Found 934.1586.

Compound **20**. Yield: 39.0%.^{1}H NMR (300 MHz, DMSO-d_6) δ 8.98 (s, 1H), 8.32 (s, 3H), 8.03 (d, J = 28.2 Hz, 1H), 7.59 (d, J = 15.7 Hz, 2H), 7.14 (t, J = 20.0 Hz, 1H), 7.02 (s, 2H), 6.29 (s, 2H), 4.34 (s, 2H), 3.85 (s, 9H), 3.82 (s, 3H), 2.66 - 2.55 (m, 2H), 2.39 - 2.22 (m, 4H), 2.11 -1.92 (m, 2H), 1.801-1.68 (m, 2H), 1.55-1.30 (m, 4H), 1.18-1.04 (m, 2H).^{13}C NMR (75 MHz, DMSO-d_6) δ 180.44, 171.38, 164.11, 163.75, 161.41 (C×2), 160.73, 150.00, 133.38, 127.76, 124.95, 124.00(C×2), 121.07, 111.27, 103.01, 91.40 (C×2), 62.00, 61.78, 60.27, 56.52 (C×2), 56.22, 56.10, 36.40, 35.77, 31.40, 31.04, 23.97 (C×2), 21.95. HR-MS (*m/z*) (ESI): calcd for $C_{32}H_{42}ClN_3O_{13}PtS$, [M-H]: 938.1700; Found 938.1862.

Compound **21**. Yield: 39.0%.^{1}H NMR (300 MHz, DMSO-d_6) δ 9.61 (s, 1H), 8.99 (s, 1H), 8.12 (s, 1H), 8.00 (s, 1H), 7.77 (s, 1H), 7.59 (d, J = 15.5 Hz, 1H), 7.41 (s, 1H), 7.11 (d, J = 15.9 Hz, 1H), 7.02 (s, 2H), 6.30 (s, 2H), 4.34 (s, 2H), 3.85-3.82 (m, 9H), 3.83 (s, 3H), 2.35-2.30 (m,

4H), 2.12-2.09 (m, 3H), 1.52-1.35 (m, 8H), 1.24 (s, 1H), 1.16 – 0.96 (m, 2H).^{13}C NMR (75 MHz, DMSO-d_6) δ 181.21, 175.25, 171.48, 164.18, 163.64, 161.42 (C×2), 150.08, 133.45, 127.68, 127.50, 124.97, 124.03, 121.08, 111.26, 103.12, 91.42 (C×2), 62.02, 61.87, 60.48, 56.53 (C×2), 56.23, 56.09, 36.68, 36.11, 31.41, 31.08, 25.41 (C×2), 25.14, 24.09. HR-MS (*m/z*) (ESI): calcd for $C_{33}H_{44}ClN_3O_{13}PtS$, [M-H]: 952.1857; Found 952.2023.

Compound **22**. Yield: 27.8%.^{1}H NMR (300 MHz, DMSO-d_6) δ 8.94 (s, 1H), 8.01 (s, 1H), 7.59 (d, *J* = 15.6 Hz, 1H), 7.11 (d, *J* = 15.6 Hz, 1H), 7.13-7.02 (m, 2H), 6.29 (s, 2H), 6.39 – 5.89 (m, 6H), 4.34 (s, 2H), 3.84 (d, *J* = 7.2 Hz, 9H), 3.83 (s, 3H), 2.43-2.39 (m, 2H), 2.31-2.27 (m, 2H), 1.79-1.77 (m, 2H).^{13}C NMR (75 MHz, DMSO-d_6) δ 180.49, 171.93, 164.23, 161.24 (C×2), 149.99, 133.21, 127.59, 127.49, 124.90, 124.33, 121.30, 110.95, 103.31, 91.15（C×2), 60.10, 56.56 (C×2), 56.24, 56.13, 36.10, 35.96, 22.18. HR-MS (*m/z*) (ESI): calcd for $C_{24}H_{34}Cl_3N_3O_9PtS$, [M-H]: 840.0637; Found 840.0766.

Compound **23**. Yield: 29.4%.^{1}H NMR (300 MHz, DMSO-d_6) δ 8.99 (s, 1H), 8.01 (s, 1H), 7.58 (d, *J* = 15.7 Hz, 1H), 7.11 (d, *J* = 15.6 Hz, 1H), 7.07 – 6.95 (m, 2H), 6.52 – 5.90 (m, 8H), 4.34 (s, 2H), 3.85 (s, 9H), 3.82 (s, 3H), 2.38-2.34 (m, 2H), 2.26-2.24 (m, 2H), 1.60-1.48 (m, 4H).^{13}C NMR (75 MHz, DMSO-d_6) δ 180.93, 171.72, 164.11, 161.43(C×2), 149.83, 133.31, 127.81, 127.46, 124.91, 123.91, 120.99, 111.14, 103.06, 91.23(C×2), 60.32, 56.55(C×2), 56.25, 56.12, 36.52, 36.28, 25.52, 25.18. HR-MS (*m/z*) (ESI): calcd for $C_{25}H_{36}Cl_3N_3O_9PtS$, [M-H]:855.0815; Found 854.0934.

Compound **25**. To a solution of compound **8** (1.50 g, 3.81 mmol) in DMF (15 mL) was added K_2CO_3 (1.3g, 9.52 mmol) and compound **24** (2.55 g,15.24 mmol), then the solution was stirred at 50 ℃for 3h . Process of the reaction was monitored by TLC. After the completion of reaction, the solvent was removed under reduced pressure, then DCM (250 mL) was added to dissolve the residue and washed with water and sat. NaCl (3×100 mL). The organic layer was dried with anhydrous Na_2SO_4 and concentrated under reduced pressure. The crude product was purified with silica gel chromatography with the eluent of DCM and EA (100:0-100:1) to get white solid 1.51 g. Yield 83.3 %. ^{1}H NMR (400 MHz, DMSO-d_6) δ 7.56 (d, *J* = 15.7 Hz, 1H), 7.10 (d, *J* = 15.7 Hz, 1H), 6.81 (d, *J* = 8.2 Hz, 1H), 6.59 (dd, *J* = 8.2, 1.8 Hz, 1H), 6.39 (d, *J* = 1.8 Hz, 1H), 6.30 (s, 2H), 5.25 (s, 1H), 4.26 (s, 2H), 4.09 (q, *J* = 7.1 Hz, 2H), 3.85 (d, *J* = 2.6 Hz, 9H), 3.81 (d, *J* = 5.9 Hz, 5H), 1.19 (t, *J* = 7.1 Hz, 3H).

Compound **26**. To a solution of compound 25 (1.50 g, 3.12mmol) in EtOH (10 mL) and pure water (5 mL) was added LiOH•H_2O (327.6 mg, 7.82 mmol) at room temperature and stirred at the same temperature for 3 h. Progress of the reaction was monitored by TLC. The reaction was worked up with removal the solvent under reduced pressure after the completion of the reaction and obtained pale yellow solid. Pure water (30 mL) was added to dissolve the residue and adjusted the pH of the solution to 5 with HCl (1M). The residue was filtered and dried at 45 ℃ to give white solid (1.2 g). Yield 85.0%.^{1}H NMR (400 MHz, DMSO-d_6) δ 12.71 (s, 1H), 7.56 (d, J = 15.7 Hz, 1H), 7.12 (d, J = 15.7 Hz, 1H), 6.78 (d, 8.1 Hz, 1H), 6.59 (dd, J = 8.1, 1.6 Hz, 1H), 6.42 (d, J = 1.6 Hz, 1H), 6.30 (s, 2H), 5.77 (s, 1H), 4.27 (s, 2H), 3.85 (s, 9H), 3.80 (s, 3H), 3.72 (s, 2H). HR-MS (*m/z*) (ESI): calcd for $C_{21}H_{25}NO_8S$, [M-H]: 450.1228; Found 450.1272.

(4) General Procedures for Preparing Compounds 27-29.

Compound **26** (0.33 mmol), compound **15,16** or **17** (0.37 mmol), TBTU (0.50 mmol) and Et_3N (0.50 mmol) in DMF (3 mL) was used for preparing compounds **17-29** following the general procedure of synthesis of compounds **18-23**.

Compound **27**. Yield: 18.8%. ^{1}H NMR (400 MHz, DMSO-d_6) δ 9.28 (d, J = 9.2 Hz, 1H), 8.19 (s, 1H), 7.87 (s, 1H), 7.53 (d, J = 15.6 Hz, 2H), 7.12 (d, J = 15.6 Hz, 1H), 6.79 (d, J = 8.0 Hz, 1H), 6.58 (d, J = 8.0 Hz, 1H), 6.45 (s, 1H), 6.29 (s, 2H), 5.20 (s, 1H), 4.33-4.21 (m, 2H), 3.86 (s, 9H), 3.79 (s, 5H), 2.74 (s, 1H), 2.08 (m, 2H), 1.57 – 1.39 (m, 3H), 1.32 – 0.98 (m, 3H), 0.91-0.87 (m, 1H).^{13}C NMR (100 MHz, DMSO-d_6) δ 180.51, 164.19, 161.37 (C×2), 146.91, 137.54, 133.10, 124.02, 121.87, 119.47, 112.81, 109.96, 103.05, 91.46 (C×2), 63.91, 62.80, 60.69, 56.61 (C×2), 56.11, 55.92, 47.33, 31.40, 31.32, 23.93 (C×2). HR-MS (*m/z*) (ESI): calcd for $C_{27}H_{38}Cl_3N_3O_8PtS$, [M-H]: 864.1060; Found 864.1065.

Compound **28.** Yield: 19.2%. ^{1}H NMR (400 MHz, DMSO-d_6) δ 8.34 (d, J = 5.8 Hz, 1H), 8.26 (d, J = 5.8 Hz, 1H), 8.05 (t, J = 9.9 Hz, 1H), 7.66 (t, J = 9.9 Hz, 1H), 7.58 (d, J = 15.7 Hz, 1H), 7.12 (d, J = 15.7 Hz, 1H), 6.78 (d, J = 8.1 Hz, 1H), 6.57 (dd, J = 8.1, 1.3 Hz, 1H), 6.44 (d, J =1.3 1H), 6.29 (s, 2H), 5.11 (t, J = 5.5 Hz, 1H), 4.35 – 4.23 (m, 2H), 3.85 (s, 9H), 3.78 (s, 5H), 2.56-2.53 (m, 1H), 2.47-2.44 (m, 1H), 2.08-2.05 (m, 1H), 1.98-1.95 (m, 1H), 1.60 – 1.40 (m, 3H), 1.35-1.27 (m, 1H), 1.15 – 0.97 (m, 2H).^{13}C NMR (100 MHz, DMSO-d_6) δ 177.49, 164.07, 163.87, 161.39 (C×2), 146.88, 143.04, 137.43, 133.09, 124.18, 121.77, 119.55, 112.72, 110.01, 103.06,

91.44 (C×2), 62.13, 61.50, 60.67, 56.53 (C×2), 56.10, 55.89, 46.81, 31.33, 31.00, 23.95 (C×2). HR-MS (*m/z*) (ESI): calcd for $C_{29}H_{38}ClN_3O_{12}PtS$, [M-H]: 882.1437; Found 882.1515.

Compound **29.** Yield: 21.2%.^{1}H NMR (400 MHz, DMSO-d_6) δ 7.56 (d, *J* = 15.7 Hz, 1H), 7.12 (d, *J* = 15.7 Hz, 1H), 6.78 (d, *J* = 8.2 Hz, 1H), 6.56 (dd, *J* = 8.2, 1.6 Hz, 1H), 6.49 (d, *J* = 1.6 Hz, 1H), 6.24 (m, 8H), 4.94 (t, *J* = 5.1 Hz, 1H), 4.28 (s, 2H), 3.86-3.85 (m, 9H), 3.78 (s, 3H), 3.74 (d, *J* = 5.0 Hz, 2H).^{13}C NMR (101 MHz, DMSO-d_6) δ 177.53, 164.05, 161.37 (C×2), 146.72, 137.50, 133.11, 124.02, 121.99, 119.35, 113.05, 109.80, 103.03, 91.46 (C×2), 60.88, 56.64 (C×2), 56.12, 55.91, 46.59. HR-MS (*m/z*) (ESI): calcd for $C_{21}H_{30}Cl_3N_3O_8PtS$, [M-H]: 784.0374; Found 784.0453.

(5) Cell Culture. All adherent cells used in this article were cultured in a humidified atmosphere of 5% CO_2 and 95% air at 37.0 °C, including A549 (non-small cell lung cancer cell line), MGC-803 (gastric cancer cell line), SKOV-3 (ovarian cancer cell line), NCI-H460 (large cell lung cancer cell line), A549/CDDP (cisplatin-resistant non-small cell lung cancer cell line), A549/DOX (doxorubicin-resistant non-small cell lung cancer cell line), SKOV-3/CDDP (CDDP-resistant ovarian cancer cell line), HEUVC (human umbilical vein endothelial cells). The cells were grown monolayer in DMEM supplemented with 10% fetal bovine serum, penicillin (100 μg/mL) and streptomycin (100 μg/mL) solution. The A549/CDDP, A549/DOX and SKOV-3/CDDP cells were constructed following the method reported previously [46,47]. Briefly, A549/CDDP or SKOV-3/CDDP cell lines survived intermittently by exposure to 8, 20, or 40 μM cisplatin in monolayer culture. Initially, A549 or SKOV-3 cell lines were co-incubated with cisplatin at a concentration of 3 nM and were continuously exposed at the same concentration of cisplatin three times for 3-day periods during a 3-6-week period. Those cell lines were allowed for growth recovery between cycles. Upon the completion of three or four cycles of drug, the concentration of cisplatin was doubled and repeated the procedure during the following long period until the noted drug levels were achieved. To verify the success of the construction of cisplatin-resistant cells, MTT assays were carried out to detect the resistance factor (RF) of cisplatin until reached experimental requirements. Similarly, A549/DOX were obtained with the same method provided above, using 0.002 μg/mL and 0.2 μg/mL as initial and final concentration respectively.

(6) In Vitro Cytotoxicity Test of Compounds. The cytotoxicity of compounds synthesized

in this article was tested with MTT methods. A549, MGC-803, SKOV-3, NCI-H460, HUVEC, A549/CDDP, A549/DOX and SKOV3/CDDP were grown on 96-well plates at a cell density of 1 × 10^5 cells/mL/well and incubated at an atmosphere of 5% CO_2 and 95% air at 37.0 °C for overnight. After that, compounds dissolved in DMF and diluted to various concentrations with medium were added to those different cells culture medium respectively. After 72 h treatment, the incubation was work up by the addition of MTT (5 mg/mL). Then, the cells were incubated for another 4h. Finally, the medium was replaced with DMSO (150 μL), the O.D. Value was read at 570/630 nm enzyme labeling instrument. The IC_{50} value of each compound was calculated by SPSS software with three parallel experiments.

(7) The Release of Compound 26 under the Reduction of Ascorbic Acid, the Stability of 29 at Acidic Condition and in A549 Cells. The stability or reduction reaction at different atmosphere was detected with RP-HPLC (waters, 2545 system). The stability of Pt(IV) was prepared a solution of compound **29** (2.0 mg, 0.5 mM) in PBS (PH= 7.4) and acetonitrile (5 mL, 90:10, V/V). The reduction of Pt(IV) was a mixture of compound **29** (2.0 mg, 0.5 mM) and ascorbic acid (1.3 mg, 1.5 mM) in PBS (PH= 7.4) and acetonitrile (5 mL, 90:10, V/V). All the solutions were preserved at 37 °C water bath in dark, detected and recorded by RP-HPLC on ODS column (250×4.6 mm, 5 μm) at different time points with an eluent of acetonitrile/water (45:55, v/v) (0.1% trifluoroacetic acid in water). Similarly, compound **26** and ascorbic acid was used as control to match the peaks of compound **29** in reduction atmosphere. The flow rate was 1.0 mL/min and the volume of sample injection was more than 20.0μL. All of the compounds tested with RP-HPLC were purified with 0.45μm filter. The wavelength for testing was 254 nm. Besides，the stability of **29** under acidic condition was also investigated by using a solution of **29** (0.5 mg) in PBS (pH = 5.5) and acetonitrile (5 mL, 90:10, V/V) and was incubated at 37 °C water bath in dark for 36 h. The results were detected and recorded with RP-HPLC (waters, e2695 system; 2489 UV/Vis detector) on ODS column (250×4.6 mm, 5 μm), using wavelength of 254 nm and an eluent of acetonitrile/water (45:55, V/V) (0.05% trifluoroacetic acid inwater).

The release of **26** from **29** in A549 cells was also conducted. Briefly, A549 cells were co-incubated with **29** (2 μM, 5 μM, 10 μM) for 24 h, washed with PBS and lysed to obtain cell lysates. Supernatant fraction gained after centrifugation was filtered with microporous filter membrane (0.22 μm), recorded and analyzed with RP-HPLC (waters, e2695 system; 2489 UV/Vis

detector). The other conditions of HPLC were the same as description mentioned above.

(8) Cellular Uptake Assay. The content of cellular uptake of CDDP and **29** was measured on A549 cells. Briefly, A549 cells were seeded in 96-well plates until reached about 80% confluence and then incubated with **29** (5 μM and 10 μM) and CDDP (5 μM and 10 μM) at 37 °C in standard culture conditions. After 12 h co-incubation, the cells were harvested, washed with ice cold PBS (3×3 mL), centrifuged at 1000 g and resuspended in PBS (1 mL). The cell numbers were counted by using 100 μL suspension, and the rest cells were digested with 65% nitric acid for ICP-MS to obtain the platinum content.

(9) Co-Immunoprecipitation. To investigate the effect of **29** on the signaling transduction between RAS and RAF, co- immunoprecipitation assays were carried out. Briefly, A549 cells (at a density of 2×10^6 cells/mL) were seeded in 6-well plates and incubated for overnight. Then the cells were co-incubated with the same concentration (5 μM) of **26** and **29**, respectively. After 24 h treatment, cells were harvested, washed with fresh ice PBS, treated with trypsin and lysed in lysis buffer (KGP701, KeyGEN BioTECH). Subsequently, the clarified cell lysates were divided into two groups of input group and IP group. The lysates of input group were subjected to western blot, following the method in 4.16. As for IP group, lysates were incubated with VE-cadherin (contains primary antibody) at 4 ^{o}C for overnight. The resulting proteins were precipitated with protein G agarose and co-incubated 4 ^{o}C for 3 h. The protein sediment obtained after centrifugation was washed with cold PBS buffer, resolved with 1XSDS-PAGE and subjected to western blot analysis according to the method mentioned in 4.12, using the indicated antibodies. The co-immunoprecipitation assays of CRAF and BRAF were carried out following the illustrations mentioned above, using CRAF antibody (Genetex, GTX 24767) and BRAF antibody (abcam, Ab33899).

(10) Microscale Thermophoresis. H-Ras protein (Sino Biological Inc.), K-RAS (Sino Biological Inc.), N-RAS (Sino Biological Inc.) and human recombinant Raf-1-RBD (EMD Millipore) were used for microscale thermophoresis (MST) assays. Firstly, H-RAS, K-RAS and N-RAS proteins were N-terminally labeled using the Monolith NT Protein Labeling Kit RED-NHS (NanoTemper Technologies, München, Germany), following the illustrations of manufacturer. And the CRAF was labeled with FITC by FITC-OSu in PBS (PH=7.4) solution and the protein eluted in 0.5ml of binding buffer (25mM Tris-HCl, pH 8.0/ 300mM NaCl) [8a].

To carried out the MST assays **26** (5 μM to 0.000153 μM) or **29** (5 μM to 0.000153 μM), K-/H-/N-RAS (100 nM) were co-incubated for 30 min at room temperature in binding buffer (25mM Tris-HCl, pH 8.0/300 mM NaCl) [8e]. Then, the binding data were recorded and analyzed with Monolith NT.115 (Nano Temper Technologies).

(11) Cellular Thermal Shift Assay. To verify that **29** interacted with CRAF protein rather than RAS, cellular thermal shift assays were performed. Briefly, A549 cell lysates were divided equally into PCR tubes and co-incubated with **26** (5 μM), **29** (5 μM) and DMF at room temperature for 30 min. Thereafter, the complexes were divided equally (20 μL) into PCR tubes and heated at the temperature ranged from 47-67 ^{o}C for 5 min. The lysates obtained after centrifugation were subjected to western blotting to analyze the stability of RAS and CRAF proteins with the antibodies in material.

(12) Cell Apoptosis Analysis. A549 cells (2×10^6 cells/mL) in the DMEM medium with 10% FBS were seeded in 6-well plates and allowed to adhere overnight. After incubation overnight, the tumor cells were treated with different compounds, namely compound **26** (5 μM), compound **29** (5 μM), cisplatin (5 μM), and vehicle (DMF) for 24 h. Then, the cells were collected and washed twice with PBS followed by the additon of 1×Binding Buffer (2×10^6 cells/mL) to resuspend the cells. The cells were treated with 5 μL AnnexinV-FITC (BD, Pharmingen) and 5 μL PI using annexin-V FITC apoptosis kit and incubated at RT in dark for 20 min and centrifuged. The apoptosis value was obtained with system software (Cell Quest; BD Biosciences). As for the cell apoptosis analysis of **26**, **29** and CDDP at IC_{50} concentration, the concentration of each compound was change to 83 nM, 6 nM and 8.2 μM and recorded the results after 72 h co-incubation with A549 cells following the illustration mentioned above.

(13) Cell Cycle Arrest Analysis. A549 cells (2×10^6 cells/mL) in the DMEM medium with 10% FBS were seeded in 6-well plates and allowed to adhere overnight. After incubation overnight, the tumor cells were treated with different compound: compound **26** (5 μM), compound **29** (5 μM), CDDP (5 μM), and vehicle (DMF) for 24 h. Then, the cells were collected and washed twice with ice-cold PBS and fixed with ice-cold ethanol at -20 °C overnight. After that, the cells were washed twice with cold PBS and treated with RNase A (100 μg /mL) at 37 °C for 20 min, centrifuged and collected. The cells were then stained with propidium iodide (1mg/mL) in dark at 4 °C for 30 min following the instructions of test kit, and analyzed with system software (Cell

Quest; BD Biosciences).

(14) Comet Assay. Human lung cancer A549 cells (2×10^6 cells/mL) were incubated in six-well plates and allowed to coherent overnight, then treated with various compound: vehicle (DMF), CDDP (5 μM), **26** (5 μM) and **29** (5 μM). After 24 h co-incubation with various compounds mentioned above, Molten LM Agarose (Trevigen) at a ratio of 1/10 (v/v) was added and transferred onto Comet Slide (Trevigen) and incubated for another 10 min at 4 °C in dark. After that, the slides were firstly immersed in lysis buffer for 30 min at 4 °C before incubated in alkaline unwinding solution (1 mM EDTA, 200 mM NaOH) for 20 min at room temperature. Finally, the slides were washed with water and 70% ethanol, dried and used for laser confocal microscope analysis.

(15) Reactive Oxygen Species Active Oxygen Analysis. Human lung cancer A549 cells (2×10^6 cells/mL) were incubated in six-well plates and allowed to coherent overnight, then treated with various compound: vehicle (DMF), CDDP (5 μM), **26** (5 μM) and **29** (5 μM). After 24 h treatment, the cells were collected at 2000 rpm and washed twice with ice PBS. Subsequently, the tumor cells were incubated with DCFH-DA (Molecular Probe, Beyotime, Haimen, China) in dark at 37 °C for 30 min, following the instructions of kit. Finally, cellular fluorescence was observed and recorded with fluorescence microscope. The colocation analyses of ROS and mitochondria were conducted as illustrated above, while using DCFH-DA and Mitochondrion Red (KEYGEN BIOTECH, KGMP0071) as probes.

(16) Mitochondrial Membrane Potential Analysis Induced by 26 and 29. Human lung cancer A549 cells (2×10^6 cells/mL) were incubated in six-well plates and allowed to coherent overnight, then treated with various compound: vehicle (DMF), CDDP (5 μM), **26** (5 μM) and **29** (5 μM). After 24 h treatment, the medium was replaced followed by staining with JC-1 fluorescent probe prepared previously according to the instructions of test kit. After 30 min treatment in dark at 37 °C, cells were collected at 2500 rpm and washed twice with new ice PBS, then the effects of various compounds on MMP of tumor cells were analyzed with flow cytometer using 530nm, 590 nm and 488 nm as emission fluorescence and excitation wavelength, respectively.

(17) Cell Morphology of Apoptosis Induced by 26 and 29. (AO and EB Co-Staining). A549 cells (2×10^6 cells/mL) in the DMEM medium with 10% FBS were seeded in 6-well plates and allowed to adhere overnight. After incubation overnight, the tumor cells were treated with

different compound: compound **26** (5 μM), compound **29** (5 μM), CDDP (5 μM), and vehicle (DMF) for 24 h. After that, the cells were washed twice with cold PBS and treated with RNase A (100 μg /mL) at 37 °C for 20 min. The cells were resuspended with treatment of trypsin (20 μL), then transferred to glass substrates and co-stained with AO (6 μg/mL) and EB (6 μg/mL) following the instructions of test kit. Finally, morphology of the cells treated with different compounds was observed and recorded with fluorescence microscope.

(18) Regulated Proteins Analyzed by Western Blotting. Human lung cancer A549 cells (2×10^6 cells/mL) were incubated in six-well plates and allowed to coherent overnight, then treated with various compounds: vehicle (DMF), CDDP (5 μM), **26** (2 μM, 5 μM) and **29** (2 μM, 5 μM). After 48 h treatment, cells were collected, centrifuged and washed twice with cold PBS. Then the cells pellet harvested was lysed with a lysis buffer on ice for 30 min, centrifuged at 15000 rpm for 15 min at 4 °C and collected. Protein amount of the cell lysates were measured with BCA protein assay reagents (Imgenex, USA) under the instructions of manufacture. Equal amounts of cellular protein lysed was separated on SDS-PAGE on 12% gels and transferred to PVDF Hybond-P membrane (GE Healthcare). Then the membrane was blocked with 5% nonfat milk in Tris-buffered saline with Tween 20 (TBST) buffer and co-incubated with primary antibodies (anti-Bcl-2, anti-Bax, anti-Cyt c, anti-Pro-caspase-9, anti-caspase-9, anti-Pro-caspase-3, anti-caspase-3, anti-Total-PARP, anti-cleaved PARP, anti-β-actin, anti-GAPDH, anti-MEK, anti-p-MEK, anti-ERK, anti-p-ERK, anti-γH2AX, anti-p53, anti-BRAF and anti-Pin1) at 4 °C for overnight. Subsequently, the membrane was incubated with second antibodies conjugated with peroxidase for 2h, washed three times with TBST buffer for 15 min and visualized with chemiluminescence reagent (Thermo Fischer Scientifics Ltd.).

(19) UV−Vis and Fluorescence Emission Detection. Compounds **26** or **29** (1.0 mg) was dissolved in acetonitrile (200 μL) and diluted to 5 μM with PBS (pH 7.4) or DMEM (10% in PBS 7.4) solution. And the CDDP was dissolved in water or DMEM (10% in PBS 7.4) to a final solution (5 μM). Then the UV absorption of the samples was recorded on a Shimadzu UV2600 instrument with wavelength ranging from 190 to 450 nm. The fluorescence emission was recorded with Shimadzu RF-6000 instrument with the excitation wavelength of 315 nm (wavelength of maximum absorption), 494 nm (wavelength of excitation wavelength) and 535 nm (wavelength of PI-DNA complexes).

(20) In Vivo Anti-Tumor Activity Assay. The mice used in in vivo experiments were purchased from Shanghai Slac Laboratory Animal Co., Ltd. (China), housed in the facility at the Laboratory Animal Center, Academy of Simcere according to the guidelines approved for laboratory animals. All surgical interventions and postoperative animal care procedures were approved by the Experimental Animal Ethics Committee of Southeast University (Nanjing, China).

To investigate the anti-tumor activity of compound **29**, A549 in vivo xenograft tumor models were utilized following the method described previously [32-34]. Briefly, 3×10^6 A549 cells in 100 μL of sterile PBS were injected subcutaneously in flank of female BALB/c athymic nude mice of 5-6 weeks of age, which were purchased from Shanghai Slac Laboratory Animal Co., Ltd. (China). After allowing the tumors reached to 150-250 mm^3, animals were assigned to four groups (three animals per group) randomly for efficacy studies and treated via injecting intravenously through tail vein with compound 29 (6 μmol/kg, on days 0, 2 and 4), Rigosertib (6 μmol/kg, on days 0, 2 and 4), CDDP (6 μmol/kg, on days 0, 2 and 4) and vehicle (equivalent volume of normal saline injection, on days 0, 2 and 4), respectively. Compound **29** was dissolved in a mixture of 0.1% Tween-80 and 2.5% DMF and diluted in saline for desired concentration. Tumor volumes and body weights were measured 2-3 times a week. Tumor volumes were obtained by measuring the perpendicular diameter of tumor in length and width and calculated according to the formula: Tumor volume (mm3) = 1/2 × length × $width^2$. Curves of tumor growth and body weights were plotted using the average data at the same group by origin 9.0.

ANCILLARY INFORMATION

Supporting Information

The Supporting Information is available free of charge on the ACS Publications website at DOI: .

Table of IC_{50} values *in vitro* of tested compounds against multidru-resistant cancer lines. The expression of P-glycoprotein (P-gp) in CDDP/DOX-resistant cancer cell lines. Charts of stability of compound **29**, the release of CDDP and compound **26** under reduction of ascorbic acid and under acidic condition The figure and data of standard curve of **26**. HPLC analysis on the release of **26** in A549 cells. Microscale thermophoresis (MST) assays and cellular protein thermal shift assays of **26** and **29.** Western blotting analysis of the effect on BRAF and BRAF-CRAF complex

induced by **29**. Table of IC_{50} values of **26**, **29** and CDDP at 24h. A549 apoptosis induced by **29** by IC_{50} concentration in 72h. DNA damage assays and ROS assays induced by **29**. UV and fluorescence spectra of **26** and **29**. Western blotting analysis of Pin 1protein induced by **29**. Table of antitumor activity of compound **29** on A549 xenograft models. Figures of HR-MS, ^{1}H, ^{13}C NMR spectra and HPLC chromatograms (**18-23, 27-29**). This material is available free of charge via the Internet. (PDF)

Molecular formula strings and some data. (CSV)

AUTHOR INFORMATION

Corresponding Authors

*E-mail: lei.fang@seu.edu.cn (L. Fang);

*E-mail:sgou@seu.edu.cn (S. Gou).

Author Contributions

Zhikun Liu[1] and Meng Wang[1] contributed equally to this work.

Notes

The authors declare no competing financial interest.

ACKNOWLEDGEMENTS

We thank the National Natural Science Foundation of China (Grant No. 21571033；81760626) and Priority Academic Program Development of Jiangsu Higher Education Institutions for the construction of fundamental facilities (Project 1107047002) for financial support of this study**.** We also show gratitude to KeyGen Biotech Company for co-immunoprecipitation assays. Dr. Fang is thankful to the support of the State Key Laboratory for Chemistry and Molecular Engineering of Medicinal Resources (Guangxi Normal University) (CMEMR2017-B05), “Qing-Lan” project in Colleges and Universities of Jiangsu Province, the National Science and Technology Major Foundation of China, and the Priority Academic Program Development of Jiangsu Higher Education Institutions.

ABBREVIATIONS USED

MAPK, mitogen-activated protein kinase; RAS.GDP, GDP-bound state of RAS; RAS.GTP, GTP-bound state of RAS; MEK, mitogen-activated protein kinase kinase; ERK, extracellular signal–regulated kinase; CDDP, cisplatin; TBTU, O-(benzotriazol-1-yl)-N,N,N',N'-tetramethyluronium tetrafluoroborate; DMF, N,N-dimethylformamide; DCM, dichloromethane;

IC_{50}, the half maximal inhibitory concentration; A549, non-small cell lung cancer cell line; MGC-803, gastric cancer cell line; SKOV-3, ovarian cancer cell line; NCI-H460, large cell lung cancer cell line; ABC, ATP binding cassette; A549/CDDP, CDDP resistant A549 cells; A549/DOX, doxorubicin resistant A549 cells; SKOV3/CDDP, CDDP resistant SKOV3 cells; HUVEC, human umbilical vein endothelial cells; P-gp, P-glycoprotein; RF, resistant factor; HPLC, high performance liquid chromatography; PBS, phosphate buffer saline; ICP-MS, inductively coupled plasma-mass spectrometry; MST, microscale thermophoresis; CETSA, cellular protein thermal shift assay; Kd, affinity constant; ; PI, propidium iodide; DSB, double-strand break; γH2AX, phosphorylation of H2AX; ROS, reactive oxygen species; DCHF-DA, 2,7-dichlorodi-hydrofluorescein diacetate; MMP, mitochondrial membrane potential; AO/EB, acridine orange/ethidium bromide; Cyt c, cytochrome C; Bcl-2, B-cell lymphoma-2 protein; Bax, Bcl-2 Associated X Protein; PARP, poly ADP-ribose polymerase; UV, ultraviolet; Pin1, prolyl-isomerase 1; IR, inhibition ration; TMS, tetramethylsilane; TLC, thin layer chromatography; HR-MS, high resolution mass spectrometry; NMR, nuclear magnetic resonance; DMEM, dulbecco's modified eagle medium; FACS, fluorescence-activated cell sorting; SDS-PAGE, sodium dodecyl sulfate polyacrylamide gel electrophoresis.

REFERENCES

[1] Downward, J. Targeting RAS signalling pathways in cancer therapy. *Nat. Rev. Cancer* **2003**, *3*, 11–22.

[2] Li, Z. L.; Prakash, P.; Buck, M. A "tug of war" maintains a dynamic protein–membrane complex: molecular dynamics simulations of C‐Raf RBD-CRD bound to K‐Ras4B at an anionic membrane. *ACS Cent. Sci.* **2018**, *4*, 298–305.

[3] Haling, J. R.; Sudhamsu, J.; Yen, I.; Sideris, S.; Sandoval, W.; Phung, W.; Bravo, B. J.; Giannetti, A. M.; Peck, A.; Masselot, A.; Morales, T.; Smith, D.; Brandhuber, B. J.; Hymowitz, S. G.; Malek, S. Structure of the BRAF-MEK complex reveals a kinase activity independent role for BRAF in MAPK signaling. *Cancer Cell* **2014**, *26*, 402–413.

[4] Shao, W.; Mishina, Y. M.; Feng, Y.; Caponigro1, G.; Cooke, V. G.; Rivera1, S.; Wang, Y.; Shen, F.; Korn, J. M.; Griner, L. A. M.; Nishiguchi, G.; Rico, A.; Tellew, J.; Haling, J. R.; Aversa, R.; Polyakov, V.; Zang, R.; Hekmat-Nejad, M.; Amiri, P.; Singh, M.; Keen, N.; Dillon, M. P.; Lees, E.; Ramurthy, S.; Sellers, W. R.; Stuart, D. D. Antitumor properties of RAF709, a highly

selective and potent inhibitor of RAF kinase dimers, in tumors driven by mutant RAS or BRAF. *Cancer Res.* **2018**, *78*, 1537–1548.

[5] Schubbert, S.; Shannon, K.; Bollag, G. Hyperactive Ras in developmental disorders and cancer. *Nat. Rev. Cancer* **2007**, *7*, 295–308.

[6] Prior, I. A.; Lewis, P. D.; Mattos, C. A comprehensive survey of Ras mutations in cancer. *Cancer Res.* **2012**, *72*, 2457–2467.

[7] Matallanas, D.; Crespo, P. New druggable targets in the Ras pathway? *Curr. Opin. Mol. Ther.* **2010**, *12*, 674–683.

[8] a) Athuluri-Divakar, S. K.; Carpio, V. D. R.; Dutta, K.; Baker, S. J.; Cosenza, S. C.; Basu, I.; Gupta, Y. K.; Reddy, M. V. R.; Ueno, L.; Hart, J. R.; Vogt, P. K.; Mulholland, D.; Guha, C.; Aggarwal, A. K.; Reddy, E. P. A small molecule RAS-mimetic disrupts RAS association with effector proteins to block signaling. *Cell* **2016**, *165*, 643–655. b) Weber, C. K.; Slupsky, J. R.; Kalmes, H. A.; Rapp, U. R. Active Ras induces heterodimerization of cRaf and BRaf. *Cancer Res.* **2001**, *61*, 3595–3598. c) Ritt, D. A.; Monson, D. M.; Specht, S. I.; Morrison, D. K. Impact of feedback phosphorylation and Raf heterodimerization on normal and mutant B-Raf signaling. *Mol. Cell. Biol.* **2010**, *30*, 806–819. d) Rushworth, L. K.; Hindley, A. D.; O'Neill, E.; Kolch, W. Regulation and role of Raf-1/B-Raf heterodimerization. *Mol. Cell. Biol.* **2006**, *26*, 2262–2272. e) McCarthy, M. J.; Pagba, C. V.; Prakash, P.; Naji, A. K.; Hoeven, D. V. D.; Liang, H.; Gupta, A. K.; Zhou, Y.; Cho, K. J.; Hancock, J. F.; Gorfe, A. A. Discovery of high-affinity noncovalent allosteric KRAS Inhibitors that disrupt effector binding. *ACS Omega* **2019**, *4*, 2921−2930.

[9] Brennan, D. F.; Dar, A. C.; Hertz, N. T.; Chao, W. C. H.; Burlingame, A. L.; Shokat, K. M.; Barford, D. A. Raf-induced allosteric transition of KSR stimulates phosphorylation of MEK. *Nature* **2011**, *472*, 366−369.

[10] Cox, A. D.; Fesik, S. W.; Kimmelman, A. C.; Luo, J.; Der, C. J. Drugging the undruggable RAS: mission possible? *Nat. Rev. Drug Discov.* **2014**, *13*, 828–851.

[11] Blasco, R. B.; Francoz, S.; Santamaría, D.; Cañamero, M.; Dubus, P.; Charron, J.; Baccarini, M.; Barbacid1, M. C-Raf, but not B-Raf, is essential for development of K-Ras oncogene-driven on-small cell lung carcinoma. *Cancer Cell* **2011**, *19*, 652−663.

[12] Joseph, E. W.; Pratilas, C. A.; Poulikakos, P. I.; Tadib, M.; Wang, W.; Taylord, B. S.; Halilovic, E.; Persaudf, Y.; Xing, F.; Viale, A.; Tsaih, J.; Chapmani, P. B.; Bollagh, G.; Solitf, D.

B.; Rosen, N. The RAF inhibitor PLX4032 inhibits ERK signaling and tumor cell proliferation in a V600E BRAF-selective manner. *Proc. Natl. Acad. Sci. USA* **2010**, *107*, 14903−14908

[13] Caunt, C. J.; Sale, M. J.; Smith, P. D.; Cook, S. J. MEK1 and MEK2 inhibitors and cancer therapy: the long and winding road. *Nat. Rev. Cancer* **2015**, *15*, 577−592.

[14] Rebocho, A.; Marais, R. New insight puts CRAF in sight as a therapeutic target. *Cancer Discov.* **2011**, *1*, 98–99.

[15] McCormick, F. C-Raf in KRas mutant cancers: a moving target. *Cancer Cell* **2018**, *33*, 158–159.

[16] Reddy, M. V. R.; Venkatapuram, P.; Mallireddigari, M. R.; Pallela, V. R.; Cosenza, S. C.; Robell, K. A.; Akula, B.; Hoffman, B. S.; Reddy, E. P. Discovery of a clinical stage multi kinase inhibitor sodium (E)-2-{2-Methoxy-5-[(2′, 4′, 6′-trimethoxystyrylsulfonyl)methyl] phenylamino-acetate (ON 01910.Na): synthesis, structure activity relationship and biological activity. *J. Med. Chem.* **2011**, *54*, 6254–6276.

[17] Gumireddy, K.; Reddy, M. V. R.; Cosenza, S. C.; Nathan, R. B.; Baker, S. J.; Papathi, N.; Jiang, J.; Holland, J.; Red, E. P. ON01910, a non-ATP-competitive small molecule inhibitor of Plk1, is a potent anticancer agent. *Cancer Cell* **2005**, *7*, 275–286.

[18] Ndagi, U.; Mhlongo, N.; Soliman, M. E. Metal complexes in cancer therapy – an update from drug design perspective. *Drug. Des. Devel. Ther.* **2017**, *11*, 599–616.

[19] Kang, T. S.; Wang, W.; Zhong, H. J.; Dong, Z. Z.; Huang,Q.; Mok,S. W. F.; Leung ,C. H.; Wong, V. K. W.; Ma, D. L. An anti-prostate cancer benzofuran-conjugated iridium(III) complex as a dual inhibitor of STAT3 and NF-kB. *Cancer Lett.* **2017**, *396*, 76–84.

[20] Liu, L. J.; Wang, W.; Huang, S. Y.; Hong, Y.; Li, G.; Lin, S.; Tian, J.; Cai, Z.; Wang, H. M. D.; Ma, D. L.; Leung, C. H. Inhibition of the Ras/Raf interaction and repression of renal cancer xenografts in vivo by an enantiomeric iridium(III) metal-based compound. *Chem. Sci.* **2017**, *8*, 4756–4763.

[21] Wang, Y.; Huang, H.; Zhang, Q.; Zhang, P. Chirality in metal-based anticancer agents. *Dalton Trans.* **2018**, *47*, 4017–4026.

[22] Wheate, N. J.; Walker, S.; Craig, G. E.; Oun, R. The status of platinum anticancer drugs in the clinic and in clinical trials. *Dalton Trans*. **2010**, *39*, 8113–8127.

[23] Florea, A. M.; Büsselberg, D. Cisplatin as an anti-tumor drug: cellular mechanisms of activity,

drug resistance and induced side effects. *Cancers* **2011**, *3*, 1351–1371.

[24] Rabik, C. A.; Dolan, M. E. Molecular mechanisms of resistance and toxicity associated with platinating agents. *Cancer Treat. Rev*. **2007**, *33*, 9–23.

[25] Ravera, M.; Gabano, E.; Zanellato, I.; Fregonese, F.; Pelosi, G.; Plattsc, J. A.; Osella, D. Antiproliferative activity of a series of cisplatinbased Pt(IV)-acetylamido/carboxylato prodrugs. *Dalton Trans*. **2016**, *45*, 5300–5309.

[26] Galluzzi, L.; Senovilla, L.; Vitale, I.; Michels, J.; Martins, I.; Kepp, O.; Castedo, M.; Kroemer, G.; Molecular mechanisms of cisplatin resistance. *Oncogene* **2012**, *31*, 1869–1883.

[27] Ma, L.; Ma, R.; Wang, Y.; Zhu, X.; Zhang, J.; Chan, H. C.; Chen, X.; Zhang, W.; Chiu, S. K.; Zhu, G. Chalcoplatin, a dual-targeting and p53 activator-containing anticancer Pt(IV) prodrug with unique mode of action. *Chem. Comm.* **2015**, *51*, 6301–6304.

[28] Yuan, Y.; Kwok, R. T. K.; Tang, B. Z.; Liu, B. Targeted theranostic platinum(IV) prodrug with a built-in aggregation-induced emission light-up apoptosis sensor for noninvasive early evaluation of its therapeutic responses in situ. *J. Am. Chem. Soc*. **2014**, *136*, 2546−2554.

[29] Ammar, A. A.; Raveendran, R.; Gibson, D.; Nassar, T.; Benita, S. A lipophilic Pt(IV) oxaliplatin derivative enhances antitumor activity. *J. Med. Chem.* **2016**, *59*, 9035–9046.

[30] Xu, Z.; Hu, W.; Wang, Z.; Gou, S. Platinum(IV) prodrugs multiply targeting genomic DNA, histone deacetylases and PARP-1. *Eur. J. Med. Chem.* **2017**, *141*, 211–220.

[31] Mukhopadhyay, S.; Barnés, C. M.; Haskel, A.; Short, S. M.; Barnes, K. R.; Lippard, S. J. Conjugated platinum(IV)-peptide complexes for targeting angiogenic tumor vasculature. *Bioconjugate Chem*. **2008**, *19*, 39–49.

[32] Fang, L.; Qin, X.; Zhao, J.; Gou S. Construction of dual stimuli-responsive platinum(IV) hybrids with NQO1 targeting ability and overcoming cisplatin resistance. *Inorg. Chem.* **2019**, *58*, 2191–2200.

[33] Qin, X.; Fang, L.; Chen, F.; Gou, S. Conjugation of Pt(IV) complexes with chlorambucil to overcome cisplatin resistance via a "joint action" mode toward DNA. *Eur. J. Med. Chem.* **2017**, *137*, 167–175.

[34] a) Huang, X.; Huang, R.; Gou, S.; Wang, Z.; Liao, Z.; Wang, H. Combretastatin A-4 analogue: a dual-targeting and tubulin inhibitor containing antitumor Pt(IV) moiety with a unique mode of action. *Bioconjugate Chem*. **2016**, *27*, 2132–2148. b) Hsu, C. C.; Lien, J. C.; Chang, C.

W.; Chang, C. H.; Kuo, S. C.; Huang, T. F. Yuwen02f1 suppresses LPS-induced endotoxemia and adjuvant-induced arthritis primarily through blockade of ROS formation, NFkB and MAPK activation. *Biochem. Pharmacol.* **2013**, *85*, 385–395. c) Wu, K. J.; Zhong, H. J.; Li, G.; Liu, C.; Wang, H. M. D.; Ma, D. L.; Leung, C. H. Structure-based identification of a NEDD8-activating enzyme inhibitor via drug repurposing. *Eur. J. Med. Chem.* **2018**, *143*, 1021–1027. d) Huang, Q.; Zhan, L.; Cao, H.; Li, J.; Lyu, Y.; Guo, X.; Zhang, J.; Ji, L.; Ren, T.; An, J.; Liu, B.; Nie, Y.; Xing, J. Increased mitochondrial fission promotes autophagy and hepatocellular carcinoma cell survival through the ROS-modulated coordinated regulation of the NFKB and TP53 pathways. *Autophagy* **2016**, *12*, 999–1014. e) Nishanth, R. P.; Jyotsna, R. G.; Schlager, J. J.; Hussain, S. M.; Reddanna, P. Inflammatory responses of RAW 264.7 macrophages upon exposure to nanoparticles: role of ROS-NFκB signaling pathway. *Nanotoxicology* **2011**, *5*, 502–516.

[35] Freeman, A. K.; Ritt, D. A.; Morrison, D. K. Effects of Raf dimerization and its inhibition on normal and disease-associated Raf signaling. *Mol. Cell* **2013**, *49*, 751–758.

[36] Garnett, M. J.; Rana, S.; Paterson, H.; Barford, D.; Marais, R. Wildtype and mutant B-RAF activate C-RAF through distinct mechanisms involving heterodimerization. *Mol. Cell* **2005**. *20*, 963–969.

[37] Rushworth, L. K.; Hindley, A. D.; O'Neill, E.; Kolch, W. Regulationand role of Raf-1/B-Raf heterodimerization. *Mol. Cell. Biol.* **2006**, *26*, 2262–2272.

[38] Loizou, J. I.; El-Khamisy, S. F.; Zlatanou, A.; Moore, D. J.; Chan, D. W.; Qin, J.; Sarno, S.; Meggio, F.; Pinna, L. A.; Caldecott, K. W. The protein kinase CK2 facilitates repair of chromosomal DNA single-strand breaks. *Cell* **2004**, *117*, 17–28.

[39] Rabik, C. A.; Dolan, M. E. Molecular mechanisms of resistance and toxicity associated with platinating agents. *Cancer Treat. Rev.* **2007**, *33*, 9−23.

[40] Saris1, C. P.; van de Vaart, P. J. M.; Rietbroek, R. C.; Bloramaert, F. A. In vitro formation of DNA adducts by cisplatin, lobaplatin and oxaliplatin in calf thymus DNA in solution and in cultured human cells. *Carcinogenesis* **1996**, *17*, 2763–2769.

[41] a) Chapman, C. M.; Sun, X.; Roschewski, M.; Aue, G.; Farooqui, M.; Stennett, L.; Gibellini, F.; Arthur, D.; Pérez-Galán, P.; Wiestner, A. ON 01910.Na is selectively cytotoxic for chronic lymphocytic leukemia cells through a dual mechanism of action involving PI3K/AKT inhibition and induction of oxidative stress. *Clin. Cancer Res.* **2012**, *18*, 1979–1991. b) Liu, C. Y.; Lee, C. F.;

Wei, Y. H. Role of reactive oxygen species-elicited apoptosis in the pathophysiology of mitochondrial and neurodegenerative diseases associated with mitochondrial DNA mutations. *J. Formos. Med. Assoc.* **2009**, *108*, 599–611.

[42] Dai, F.; Li, Q.; Wang, Y.; Ge, C.; Feng, C.; Xie, S.; He, H.; Xu, X.; Wang, C. Design, synthesis, and biological evaluation of mitochondria targeted Flavone−naphthalimide−polyamine conjugates with antimetastatic activity. *J. Med. Chem.* **2017**, *60*, 2071−2083.

[43] Wang, J.; Yi, J. Cancer cell killing via ROS: To increase or decrease, that is the question. *Cancer Biol. Ther*. **2008**, *7*, 1875−1884.

[44] Clerkin, J. S.; Naughton, R.; Quiney, C.; Cotter, T. G. Mechanisms of ROS modulated cell survival during carcinogenesis. *Cancer Lett*. **2008**, *266*, 30–36.

[45] Jimeno, A.; Chan, A.; Cusatis1, G.; Zhang1, X.; Wheelhouse1, J.; Solomon1, A.; Chan, F.; Zhao, M.; Cosenza, S. C.; Reddy, M. V. R.; Rudek, M. A.; Kulesza, P.; Donehower, R. C.; Reddy, E. P.; Hidalgo, M. Evaluation of the novel mitotic modulator ON 01910.Na in pancreatic cancer and preclinical development of an ex vivo predictive assay. *Oncogene* **2009**, *28*, 610–618.

[46] Bohrens, B. C.; Hamilton, T. C.; Masuda, H.; Grotzinger, K. R.; Whang-Peng, J.; Louie, K. G.; Knutsen, T.; McKoy, W. M.; Young, R. C.; Ozols, R. F. Characterization of a cis-diamrninedichloroplatinum(II)-resistant human ovarian cancer cell line and its use in evaluation of platinum analogues. *Cancer Res.* **1987**, *47*,414–418.

[47] Coley, H. M.; Amos, W. B.; Twentyman, P. R.; Workman, P. Examination by laser scanning confocal fluorescence imaging microscopy of the subcellular localisation of anthracyclines in parent and multidrug resistant cell lines. *Br. J. Cancer* **1993**, *67*, 1316–1323.

Table of Contents graphic

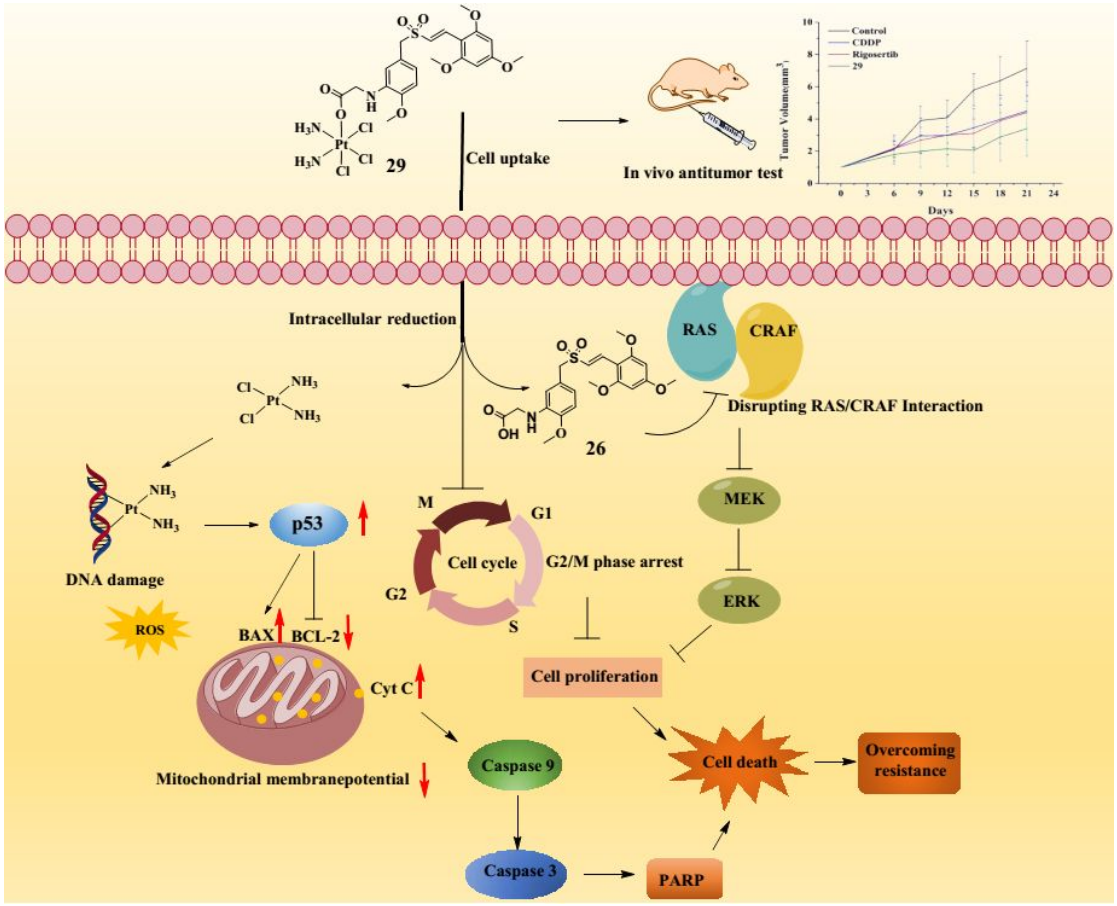

A series of styrylbenzylsulfone derivatives generated from the platinum-based modification of the side chain of Rigosertib were designed and synthesized. The most active compound **29** showed excellent antitumor activity both in vitro and in vivo due to its unique multifunctional action mode.